JOURNAL OF THE AMERICAN CHEMICAL SOCIETY
pubs.acs.org/JACS Article

Unraveling the Mechanism of Ammonia Electrooxidation by Coupled Differential Electrochemical Mass Spectrometry and Surface-Enhanced Infrared Absorption Spectroscopic Studies

Hongsen Wang, Dario R. Dekel, and Héctor D. Abruña*

Cite This: *J. Am. Chem. Soc.* 2024, 146, 15926−15940 Read Online

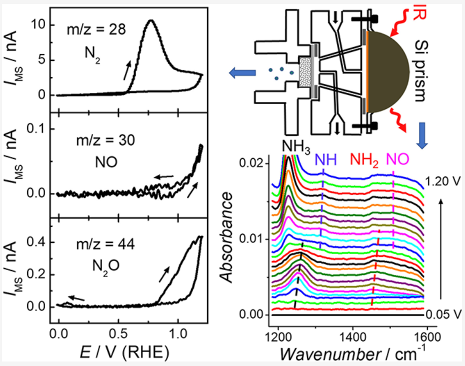

ABSTRACT: Ammonia electrooxidation has received considerable attention in recent times due to its potential application in direct ammonia fuel cells, ammonia sensors, and denitrification of wastewater. In this work, we used differential electrochemical mass spectrometry (DEMS) coupled with attenuated total reflection−surface-enhanced infrared absorption (ATR−SEIRA) spectroscopy to study adsorbed species and solution products during the electrochemical ammonia oxidation reaction (AOR) on Pt in alkaline media, and to correlate the product distribution with the surface ad-species. Hydrazine electrooxidation, hydroxylamine electrooxidation/reduction, and nitrite electroreduction on Pt have also been studied to enhance the understanding of the AOR mechanism. NH_3, NH_2, NH, NO, and NO_2 ad-species were identified on the Pt surface with ATR−SEIRA spectroscopy, while N_2, N_2O, and NO were detected with DEMS as products of the AOR. N_2 is formed through the coupling of two NH ad-species and then subsequent further dehydrogenation, while the dimerization of HNO_{ad} leads to the formation of N_2O. The NH−NH coupling is the rate-determining step (rds) at high potentials, while the first dehydrogenation step is the rds at low potentials. These new spectroscopic results about the AOR and insights could advance the search and design of more effective AOR catalysts.

1. INTRODUCTION

In recent years, the electrochemical ammonia oxidation reaction (AOR) has attracted increased attention since it can be potentially used as a green, renewable fuel for direct ammonia fuel cells (DAFCs). Ammonia is a more promising fuel than organic molecules such as methanol and ethanol due to its carbon-free nature and widely available production, storage, and transportation networks. Ammonia possesses a high energy density (18.8 MJ/kg), and thus can be used as a hydrogen storage medium, instead of pure hydrogen, since it can be easily liquified and has a very high hydrogen storage capacity (18 wt %). In addition, we believe that in the future it will be possible to generate ammonia, on-demand, by on-site, entirely carbon-free, electrolysis cells powered by renewable electricity from solar or wind sources. While the AOR on Pt group metals (PGMs) has been studied for several decades, the mechanism is still not fully understood.[1−9] So far, Pt and Ir are the most active catalysts among pure PGMs.[10] Among Pt single crystals, the Pt(100) facet is the most active.[11−13] Pt nanoparticles with preferentially (100)-oriented facets also exhibited an enhanced AOR activity when compared to poly-orientated Pt nanoparticles.[14] These studies suggest that the AOR is a surface structure-sensitive process, and almost exclusively takes place on Pt(100) facets.[14] However, (100)-oriented Pt nanoparticles still exhibit a very low activity for the AOR and suffer from surface poising. The development of next-generation catalysts has been hindered partially by the limited understanding of the mechanism of AOR. The AOR is easier to occur in alkaline media than in acidic media, so most studies of AOR have been performed in alkaline media. So far, there are two suggested AOR mechanisms including the Oswin-Salomon (O−S) mechanism and the Gerischer-Mauerer (G−M) mechanism.[1,2]

Oswin and Salomon studied the AOR kinetics on Pt for the first time and suggested a successive dehydrogenation mechanism, as shown below[1]

$$NH_3 + M + OH^- \rightarrow M{-}NH_2 + H_2O + e^- \qquad (1)$$

$$M{-}NH_2 + OH^- \rightarrow M = NH + H_2O + e^- \qquad (2)$$

$$M = NH + OH^- \rightarrow M \equiv N + H_2O + e^- \qquad (3)$$

$$M \equiv N + N \equiv M \rightarrow 2M + N_2 \qquad (4)$$

Received: February 21, 2024
Revised: April 17, 2024
Accepted: April 22, 2024
Published: May 31, 2024

https://doi.org/10.1021/jacs.4c02621
J. Am. Chem. Soc. 2024, 146, 15926−15940

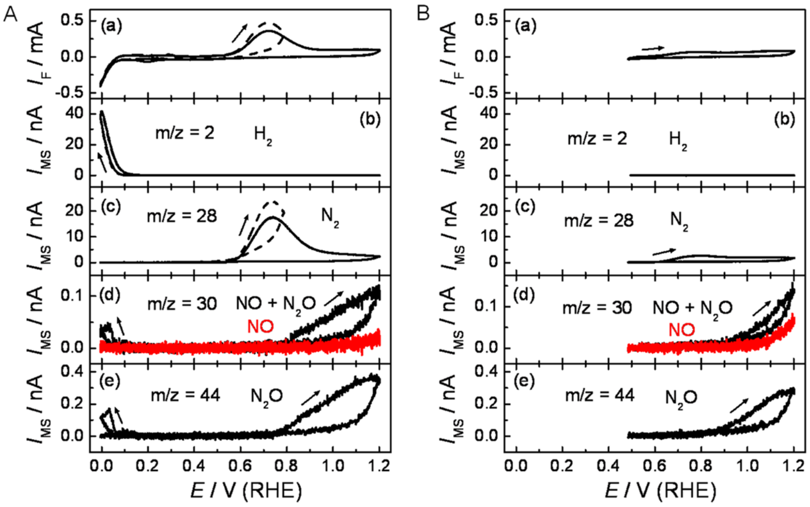

Figure 1. CVs (a) and the corresponding MSCVs of $m/z = 2$ (b), $m/z = 28$ (c), $m/z = 30$ (d), and $m/z = 44$ (e) for NH_3 oxidation on a Pt film, sputtered on a porous Teflon membrane, in the conventional DEMS cell. Electrolyte: 0.1 M NH_3 + 0.1 M KOH. Scan rate: 10 mV/s. Potential region: 0−0.8 V (A, black dashed lines), 0−1.2 V (A, black solid lines), and 0.5−1.2 V (B, black solid lines). Red lines in (d) indicate the MS signal of NO.

where M represents adsorption sites of transition metal surfaces.

Later, Gerischer and Mauerer proposed a modified mechanism involving the coupling of non-fully dehydrogenated intermediates (NH_x) and subsequent further dehydrogenation to form nitrogen, as shown below[2]

$$NH_3(aq) \rightarrow NH_{3,ad} \tag{5}$$

$$NH_{3,ad} + OH_{ad}^{(\delta-)} \rightarrow NH_{2,ad} + H_2O + \delta e^- \tag{6}$$

$$NH_{2,ad} + OH_{ad}^{(\delta-)} \rightarrow NH_{ad} + H_2O + \delta e^- \tag{7}$$

$$NH_{x,ad} + NH_{y,ad} \rightarrow N_2H_{(x+y),ad} \tag{8}$$

$$N_2H_{(x+y),ad} + (x+y)OH_{ad}^{(\delta-)} \rightarrow N_2 + (x+y)H_2O + (x+y)\delta e^- \tag{9}$$

$$NH_{ad} + OH_{ad}^{(\delta-)} \rightarrow N_{ad} + H_2O + \delta e^- \tag{10}$$

where $OH_{ad}^{(\delta-)}$ represents partially discharged adsorbed hydroxyl species, and its charge is potential-dependent.

De Vooys et al. experimentally and theoretically studied the AOR on Pt, Ir, Pd, Ru, Rh, Au, Ag, and Cu in alkaline media and proposed that the G−M mechanism was also valid for the AOR on other transition metals (TMs), i.e., NH_x ad-species were the active intermediate for the selective formation of N_2 on all TMs, whereas adsorbed nitrogen (N_{ad}) poisoned the TM surfaces. Among them, only Pt and Ir possess a good dehydrogenation capacity and a sufficiently low affinity to N_{ad}, and thus, active intermediates of $NH_{x,ads}$, which are needed for N_2 formation, can be continuously produced.[10]

Mavrikakis et al. performed density functional theory (DFT) studies of the AOR on a series of metal surfaces such as Pt, Ir, Pd, Rh, Ru, Os, Re, Ni, Co, Au, Ag, and Cu in terms of the two above-mentioned mechanisms. They found that the G−M mechanism is kinetically more favorable than the O−S mechanism and that N_{ad} poisons TM surfaces. Based on the Sabatier principle, they predicted that Pt is the most active catalyst followed by Ir and then Cu, and other TMs have very low activity.[15]

Rosca et al. compared the AOR on Pt(111) and Pt(100) and proposed that NH_2 ad-species, which are stabilized on Pt(100), act as active intermediates for the AOR and their dimerization to form hydrazine is the rate-determining step (rds) for N_2 formation.[16] In contrast, Yang et al. performed free-energy calculations of all AOR elementary steps on Pt(100) by using *ab initio* molecular dynamics and claimed that NH_3 dehydrogenation to NH_2 was the rds and that N_2 was formed through NH_2 dimerization to N_2H_4 followed by further dehydrogenation of N_2H_4.[8] However, Katsounaros et al. proposed that N_2 is formed through NH−NH coupling for the AOR.[6]

Contrarily, Skachkov et al. employed first-principles molecular dynamics and DFT calculations to study the AOR on Pt(100) and proposed that the O−S mechanism acts at moderate potentials (≥0.5 V), while the G−M mechanism turns on at low potentials (<0.5 V). They claimed that the high activity of Pt(100) could be ascribed to the facile dimerization of bridge-bonded N_{ad} to form N_2, while the low activity of Pt(111) and Pt(110) is due to strongly bound N_{ad} at hollow sites which poisons the surface.[17]

To elucidate the AOR mechanism, differential electrochemical mass spectrometry (DEMS), infrared, and Raman spectroscopies have been used to identify the products and intermediates. Besides N_2 as the major product of the AOR, DEMS results revealed that N_2O and NO are also formed on polycrystalline and single-crystalline Pt surfaces at high potentials.[5,11] NO_2^- and NO_3^- could also be formed at even higher potentials.[5] Vidial-Iglesias et al. studied the AOR on nanostructured Pt electrodes by using surface-enhanced Raman spectroscopy (SERS) and reported that the azide anion was involved in the AOR as an intermediate to form N_2.[18] De Vooys et al. revealed by SERS that N_{ad} was formed during the AOR on a Pd electrode and thus poisoned Pd.[19] Matsui et al. studied the AOR on Pt and CeO_2- and Y_2O_3-modified Pt electrodes by attenuated total reflection−surface-enhanced infrared absorption (ATR−SEIRA) spectroscopy and reported that NH_3, N_2H_4, and bridged-bonded NO

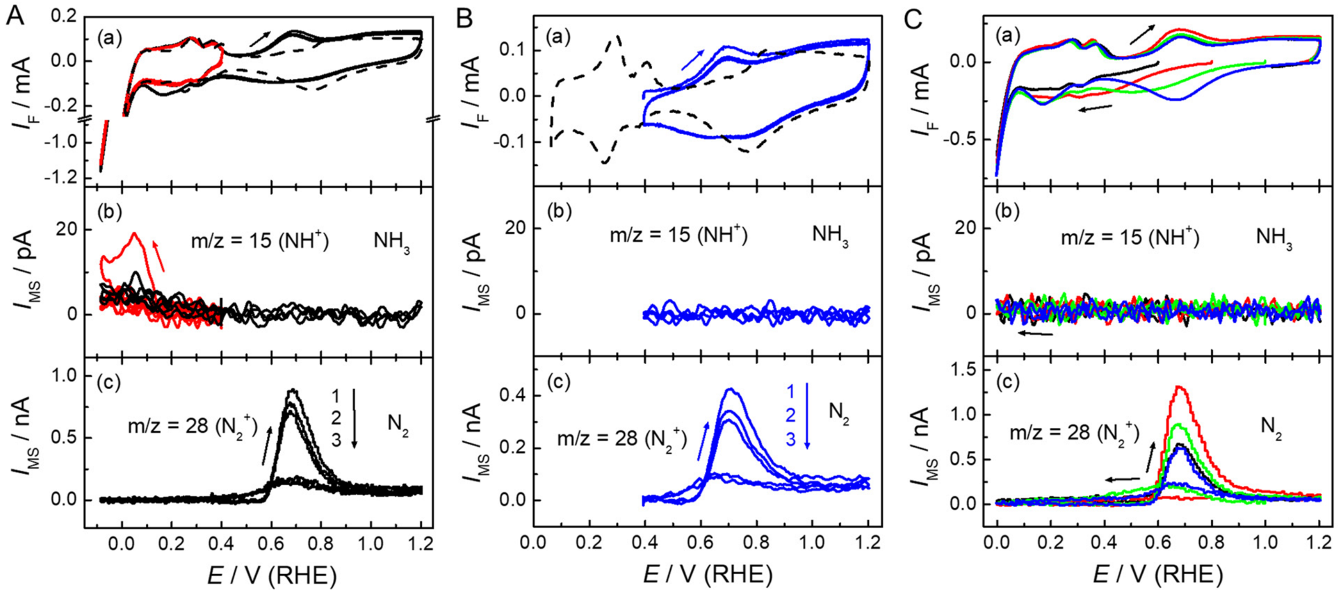

Figure 2. CVs (a) and the corresponding MSCVs of NH_3 (b) and N_2 (c) for NH_3 adsorbate stripping from a Pt film, sputtered on a porous Teflon membrane, in the conventional DEMS cell. Electrolyte: 0.1 M KOH. Scan rate: 50 mV/s. (A) Potential was first scanned between −0.1 and 0.4 V for 5 cycles (red lines), and then between −0.1 and 1.2 V (black lines). (B) Potential was scanned between 0.4 and 1.2 V (blue lines). CV of the Pt film in 0.1 M KOH is indicated by the black dashed lines. NH_3 was adsorbed at 0.4 V (A, B) and 0.6 (C, black lines), 0.8 (C, red lines), 1.0 (C, green lines), and 1.2 V (C, blue lines) from 0.1 M NH_3 + 0.1 M KOH for 5 min.

($NO_{ad,B}$) were formed as ad-species.[20−22] Using ATR−SEIRA spectroscopy, Cai et al. identified NH_3, N_2H_4, linearly, bridged, and hollow NO, bridged NO_2^-, and NO_3^- as ad-species for the AOR on an Ir electrode.[23]

Endo et al. studied the AOR on Pt by using a rotating ring-disk electrode (RRDE), and found that the peak current density decreased with increasing rotating rate and a small amount of NH_2OH was also formed at potentials of N_2 formation.[24]

NO, N_2O, NO_2^-, and NO_3^- are involved in the electrocatalytic reactions of the nitrogen cycle, and they are also involved in the AOR as reaction intermediates or products. The knowledge of their electrocatalytic reactions could advance the understanding of the AOR mechanism. The electrocatalytic reduction and oxidation mechanism of these N-containing species have also been studied.[3,25−39]

The above comprehensive literature survey clearly indicates that although the AOR has been studied by experimental and theoretical methods, the mechanisms of the AOR are not yet completely understood, especially for the N_2 formation step. There are even some contradictive statements about the AOR mechanism. In an effort to achieve a molecular-level understanding of the AOR mechanism, in this work, we employed a coupled spectroscopic platform that combined DEMS and ATR−SEIRA spectroscopy to simultaneously identify solution products and surface ad-species so that we could correlate the products in solution with surface ad-species. A detailed AOR mechanism is proposed based on our spectroscopic findings.

2. RESULTS AND DISCUSSION

2.1. Ammonia Electrooxidation. *2.1.1. DEMS Study of the AOR Under Stationary Electrolyte Condition.* Figure 1A presents the DEMS data for the AOR on a Pt film, sputtered on a porous Teflon membrane, in a conventional cell (Figure S1a) under stationary electrolyte conditions. The conventional DEMS cell was used due to its high sensitivity and fast time response, as well as the stability of the Teflon membrane when compared to a Si prism in alkaline media. Figure 1A(a) shows the cyclic voltammograms (CVs) with an upper potential limit of 0.8 and 1.2 V, while Figure 1A(b−e) displays the mass spectrometric (MS) cyclic voltammograms (MSCVs) of H_2 at $m/z = 2$, N_2 at $m/z = 28$, NO at $m/z = 30$, and N_2O at $m/z = 44$. The contributions of hydrocarbon contamination to the MS signals at $m/z = 28$, 30, and 44 were negligible (Figure S2). The AOR started at around 0.5 V and reached a maximum at ca. 0.7 V and then decreased due to the blockage by OH and/or O ad-species. N_2 started to form at ca. 0.5 V, while the formation of N_2O onset at ca. 0.75 V, where oxide species started to form on the Pt surface. The MS signal of $m/z = 30$ was mainly attributed to the NO^+ fragment of N_2O. After subtracting the contribution of NO^+ fragment of N_2O, the red line in Figure 1A(d) represents only the MS signal of NO. Only a very small amount of NO was formed at potentials of >1.0 V. The AOR on Pt generated mainly N_2, especially at potentials <0.75 V. The current efficiencies of N_2O and NO in one potential cycle, between 0 and 1.2 V, were ca. 6 and <1%, respectively. As the upper potential increased from 0.8 to 1.2 V, the peak current at 0.7 V became smaller and the Pt surface lost its activity in the reverse scan. This suggests that the Pt surface was poisoned by ad-species formed at high potentials. The poisoning species were likely N_{ad}, NO_{ad}, and $NO_{2,ad}$ (see below).[38]

As the low potential limit was increased, the AOR was significantly suppressed in the positive-going scan (Figures 1B and S3), and the MS signals of N_2 and N_2O were also suppressed. In contrast, the MS signal of NO slightly increased due to the accumulation of NO_{ad} at high potentials. As the upper potential limit went up to 1.2 V, a reductive peak emerged at ca. 0.15 V in the subsequent negative-going scan, [Figures 1A(a) and S4], while two MS peaks of N_2O appeared at potentials of <0.2 V [Figure 1A(e)]. This was ascribed to the reduction of NO_{ad} and NO_2^-, which were formed at high

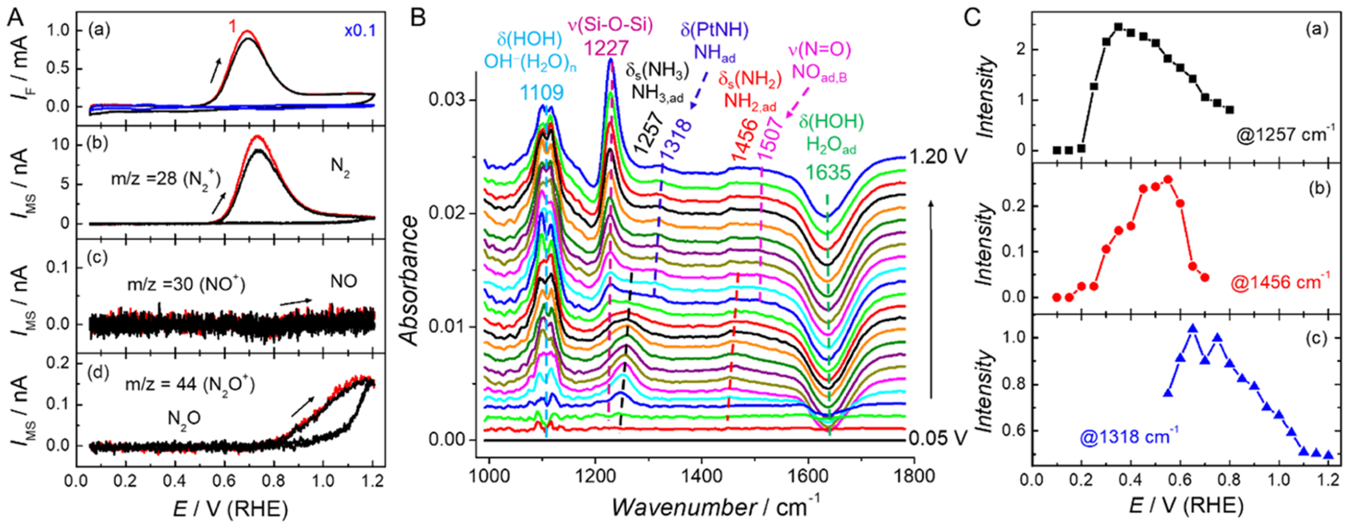

Figure 3. (A) CVs (a) and the corresponding MSCVs of N_2 (b), NO (c), and N_2O (d) for NH_3 oxidation on a Pt film, chemically deposited on a Si prism, in the dual thin-layer flow cell. Electrolyte: 0.1 M NH_3 + 0.1 M KOH. Scan rate: 5 mV/s. Electrolyte flow rate: 10 μL/s. The red lines and black lines denote the first positive-going scan and following scans, respectively. The blue line indicates the CV of the Pt film in 0.1 M KOH at a scan rate of 50 mV/s. (B) Simultaneously recorded SEIRA spectra. The reference spectrum was taken at 0.05 V. (C) Intensities of infrared bands at 1257, 1456, and 1318 cm^{-1} plotted vs potential.

potentials (Figure S5 and see below). The reduction peak around 0.15 V was mainly attributed to the reduction of NO_{ad} and NO_2^- to form NH_2OH and NH_3, since there were no corresponding signals at m/z = 28, 30, and 44.

In the CVs of AOR on Pt (Figure S4), the H adsorption peak of Pt(100) facets at ca. 0.4 V was completely blocked by NH_3 ad-species, while the H adsorption peak of Pt(110) facets at ca. 0.3 V was much less suppressed. This suggests that NH_3 decomposition/oxidation mainly takes place at Pt(100) facets, consistent with the fact that Pt(100) single crystals exhibited the highest activity for the AOR.[11−13] The redox currents at ca. 0.15 and ca. 0.5 V in the CVs for the AOR on Pt were higher than those in the blank electrolyte, indicating that NH_3 ad-species were reduced/oxidized at these potentials.

DEMS data for NH_3 ad-species stripping from the Pt film are presented in Figures 2 and S6. After NH_3 adsorption at 0.4 V from 0.1 M NH_3 + 0.1 M KOH for 5 min and subsequently exchanging the electrolyte to 0.1 M KOH, the potential was initially scanned in the negative direction. NH_3 was formed in the hydrogen region (Figure 2A), indicated by the MS signal at m/z = 15. This suggests that NH_x (x = 0−3) ad-species were formed during NH_3 adsorption at 0.4 V. In the subsequent positive-going scan, N_2 was formed at around 0.7 V. The ad-species could not be completely removed in the first positive-going scan, and many cycles were required to completely oxidize it (Figure 2A). Trace amounts of N_2O were also formed at potentials of >0.75 V (Figure S6). Upon the direct oxidative stripping of NH_3 ad-species, N_2 was also formed at potentials >0.5 V with a maximum at ca. 0.7 V (Figure 2B). NH_3 adsorption was also performed at higher potentials (Figure 2C), and the highest coverage of NH_3 ad-species was obtained at 0.8 V. The coverage of NH_3 adsorbates, estimated from the suppression of hydrogen underpotential deposition (H upd) and CO adsorption, was less than 8% (Figure S7). As NH_3 was adsorbed at 1.0 and 1.2 V, a small reduction peak appeared at ca. 0.17 V, suggesting that a small amount of NO_{ad} was formed (Figure S5).

In order to identify NH_3 ad-species on the Pt surface and to correlate the products formed in the AOR with the surface ad-species, we further performed a coupled DEMS and SEIRA spectroscopic study.

2.1.2. Coupled DEMS/ATR−SEIRA Spectroscopic Study of the AOR under Well-Defined Electrolyte Flow Conditions.

In the conventional DEMS cell (Figure S1a), the electrolyte is stationary so that the AOR products can readsorb and be reduced in the following cathodic scan. In addition, the NH_3 concentration at the electrode could be lower than the nominal one due to possible (and likely) NH_3 evaporation through the porous electrode into the vacuum. These not only complicate the analysis but may also lead to a false interpretation of the AOR mechanism. To mitigate the effects of product readsorption and successive reduction at low potentials, and to monitor surface ad-species changing with applied potential, a home-built DEMS/ATR−SEIRA spectroscopic setup was used, in which through a dual thin-layer flow cell (Figure S1b),[40,41] DEMS data and infrared spectra could be simultaneously recorded during the AOR, enabling the correlation of production formation in solution with surface ad-species.

Simultaneously recorded DEMS data and SEIRA spectra for the AOR on a Pt film, chemically deposited on a Si prism, are presented in Figure 3. The DEMS data are similar to those for a Pt film sputtered on a porous Teflon membrane, except that N_2O was not observed at potentials below 0.2 V in the negative-going scan due to the electrolyte flow. The second positive-going scan exhibited a smaller peak current than the first positive-going scan due to the poisoning by ad-species. At potentials below 0.7 V, the cathodic current, larger than that in the blank electrolyte, was attributed to the reduction of NH_x ad-species formed at high potentials.

As we increased potential from 0.05 V, several upward and downward infrared bands developed (Table S1). The band at ca. 1227 cm^{-1} is assigned to the Si−O−Si stretching ν(Si−O−Si) of SiO_2.[42] This band intensity increased with increasing potential due to the oxidation of the Si surface. The infrared band at 1257 cm^{-1}, onsetting at potentials >0.15 V, is assigned to the symmetric bending $\delta_s(NH_3)$ of adsorbed NH_3 ($NH_{3,ad}$), and had a Stark tuning rate of 39 cm^{-1}/V.[43−49] Some authors have assigned this band to the wagging $\omega(NH_2)$ of adsorbed NH_2NH_2.[20−23] It is well known that NH_2NH_2 is easily oxidized to form N_2 at potentials >0.1 V (see below). However, we did not observe the evolution of N_2 at potentials below 0.5 V using DEMS. In addition, NH_2NH_2 adsorption on Pt exhibited three infrared bands at 1270, 1360, and 1435 cm^{-1} (see below), which are different from those of $NH_{3,ad}$. Thus, this band cannot be ascribed to adsorbed NH_2NH_2. There might be an asymmetric bending $\delta_{as}(NH_3)$ of $NH_{3,ad}$ at 1600−1650 cm^{-1},[48,50,51] which was likely infrared-inactive and/or overlapped with the $\delta(HOH)$ band of water, thus preventing further analysis. The band intensity of $NH_{3,ad}$ first increased with increasing potential due to a decrease in the coverage of upd H, indicating an increase in NH_3 coverage. As the potential went up beyond 0.35 V, the band intensity of $NH_{3,ad}$ decreased (Figure 3C(a)), due to its further dehydrogenation to form adsorbed NH_2 ($NH_{2,ad}$). Another weak infrared band at 1456 cm^{-1} appeared at ca. 0.2 V and reached its maximum at around 0.5 V and then decreased with further increasing potential. We assigned this band to the symmetric bending $\delta_s(NH_2)$ of $NH_{2,ad}$.[26,39,52] It had a Stark tuning rate of 39 cm^{-1}/V. The third band at 1318 cm^{-1} appeared, as the band intensity of $NH_{2,ad}$ started to decrease and the AOR onset. We assigned this band to the bending $\delta(Pt{-}N{-}H)$ mode of adsorbed NH (NH_{ad}), rather than bridge-bonded NO_2^-,[23] since NO_2^- cannot be formed at such low potentials. It had a Stark tuning rate of ca. 24 cm^{-1}/V. This band reached a maximum at about 0.7 V and then gradually decreased. The Faradaic current also exhibited a maximum at ca. 0.7 V and was parallel to the band intensity of NH_{ad}, suggesting that NH_{ad} was the precursor for N_2 formation through dimerization. This is consistent with the finding of Pillai et al.[9] The band of NH_{ad} can be observed over a broad potential range from 1.2 V down to 0.5 V, while the N_2 formation was slow, suggesting that NH_{ad} dimerization was slow, and thus determined the rate of N_2 formation (Figure S8). A very broad and weak band at ca. 1507 cm^{-1} appeared at potentials higher than 0.6 V, which can be assigned to the stretching $\nu(NO)$ mode of $NO_{ad,B}$.[20−22,53] In contrast, this band was also assigned to the $\nu(NO)$ and/or $\delta(ONH)$ of adsorbed nitroxyl (HNO_{ad}).[51,54−57] There are still contradictions regarding this band assignment.[55,58] Another very weak band at 1338 cm^{-1} was observed in the reverse scan and is assigned to the symmetric stretching $\nu_s(NO_2)$ of adsorbed NO_2 ($NO_{2,ad}$) (Figure S8).[59,60] The upward band at 1109 cm^{-1} is assigned to the bending $\delta(HOH)$ of hydrated OH^- anion in the double layer.[42] In contrast, this band has been assigned to $\delta(PtOH)$ of adsorbed OH by numerous authors.[61] It should be noted that adsorbed OH and OH^- anion are different species. Adsorbed OH species are adsorbed on Pt through the formation of a Pt−O bond, while OH^- anion is likely present in the double layer without the formation of a Pt−O bond.[42] A band for the stretching $\nu(OH)$ of OH^- anion was observed at 3675 cm^{-1} (Figure S8). Two downward bands, observed at 1635 and 3350 cm^{-1}, are assigned to the bending $\delta(HOH)$ and the stretching $\nu(OH)$ of water (adsorbed or in the double layer), respectively.[42] Their band intensities decreased with increasing potential, opposite to the band of OH^- anion. This suggested that OH^- anions gradually displaced water in the double layer with increasing potential.

This is further confirmed by the experiment of NH_3 adsorption at a constant potential of 0.4 V (Figure 4). Upon introducing 0.1 M NH_3 into the electrolyte of 0.1 M KOH, the band intensities of OH^- (at 1109 and 3675 cm^{-1}) increased due to a higher OH^- concentration after adding ammonia, while the band intensities of adsorbed water (at 1640 and 3200 cm^{-1}) decreased. This is due to the displacement of water by OH^- in the double layer. Besides the above-mentioned bands of OH^- and water, two upward bands appeared at 1259 and 1442 cm^{-1}, respectively. They are assigned to the $\delta_s(NH_3)$ of $NH_{3,ad}$ and the $\delta_s(NH_2)$ of $NH_{2,ad}$ respectively, as mentioned above.

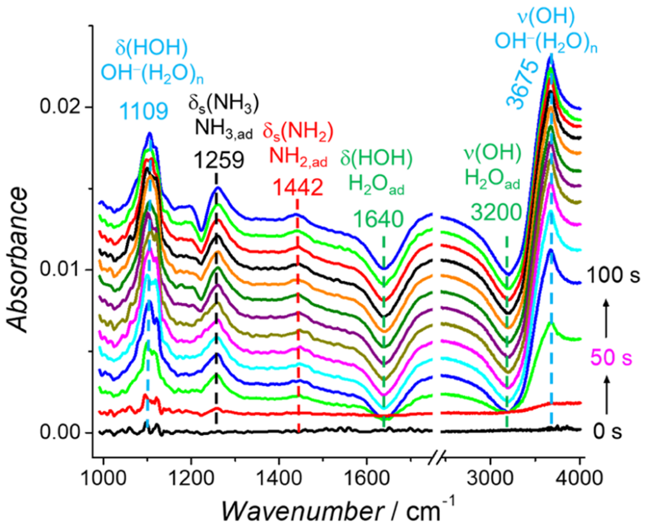

Figure 4. Time-dependent SEIRA spectra for NH_3 adsorption on a Pt film, chemically deposited on a Si prism, at 0.4 V in 0.1 M NH_3 + 0.1 M KOH in the dual thin-layer flow cell. The reference spectrum was taken at 0.4 V in 0.1 M KOH.

2.2. Hydrazine Electrooxidation on Pt.

Some authors have proposed that adsorbed NH_2NH_2 is the intermediate for the AOR on Pt.[16,20,23] To elucidate if NH_2NH_2 is the intermediate for the AOR to form nitrogen, we also carried out NH_2NH_2 electrooxidation on Pt. Figure 5A presents the CV and corresponding MSCVs of m/z = 2, 15, 28, 30, and 44 for NH_2NH_2 oxidation on a Pt film, sputtered on a porous Teflon membrane, in the conventional DEMS cell. The electrooxidation of NH_2NH_2 onset at ca. 0.1 V, and N_2 was the dominant product, as indicated by the MS signal of m/z = 28 in Figure 5A(d). A small amount of H_2 was generated, especially in both the hydrogen and oxygen regions [Figure 5A(b)]. A very small amount of N_2O was also formed at potentials of >0.2 V [Figure 5A(f)]. The MS signal of m/z = 15 is ascribed to an isotope fragment ($^{15}N^+$) of N_2, while the MS signal of m/z = 30 is attributed to an isotope fragment ($^{15}N_2^+$) of N_2 as well as the fragment (NO^+) of N_2O. During NH_2NH_2 oxidation at 0.2 V, three infrared bands appeared at 1270, 1360, and 1435 cm^{-1} (Figure 5B), which can be assigned to the bending mode $\delta(NH_x)$ of adsorbed hydrazine or partially dehydrogenated hydrazine,[43,47,49,62−64] and are very different from NH_3 adsorption.

2.3. Hydroxylamine Electrooxidation on Pt.

N_2 formation during the AOR on Pt onsets at ca. 0.5 V, where OH ad-species are present on Pt surfaces, and thus might also be involved in N−N coupling.[7] NH_2OH was also proposed to be the intermediate for the AOR on Pt.[24] NH_2OH already has a hydroxyl functional group, which allows us to study how it affects N−N coupling and products.

2.3.1. DEMS Study of Hydroxylamine Electrooxidation under Stationary Electrolyte Condition.

CVs and the

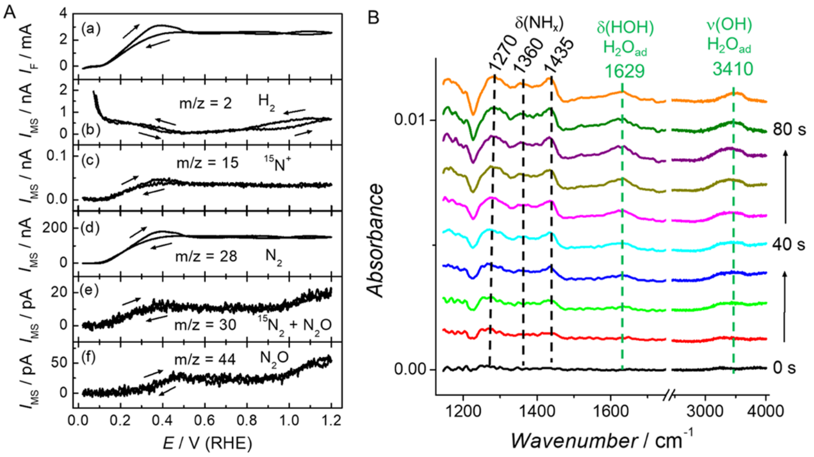

Figure 5. (A) CV (a) and the corresponding MSCVs of $m/z = 2$ (b), $m/z = 15$ (c), $m/z = 28$ (d), $m/z = 30$ (e), and $m/z = 44$ (f) for NH_2NH_2 oxidation on a Pt film, sputtered on a porous Teflon membrane, in the conventional DEMS cell. Electrolyte: 0.05 M NH_2NH_2 + 0.1 M KOH. Scan rate: 10 mV/s. (B) Time-dependent SEIRA spectra for NH_2NH_2 adsorption at 0.2 V in 0.025 M NH_2NH_2 + 0.1 M KOH on a Pt film, chemically deposited on a Si prism, in the dual thin-layer flow cell. The reference spectrum was taken at 0.2 V in 0.1 M KOH.

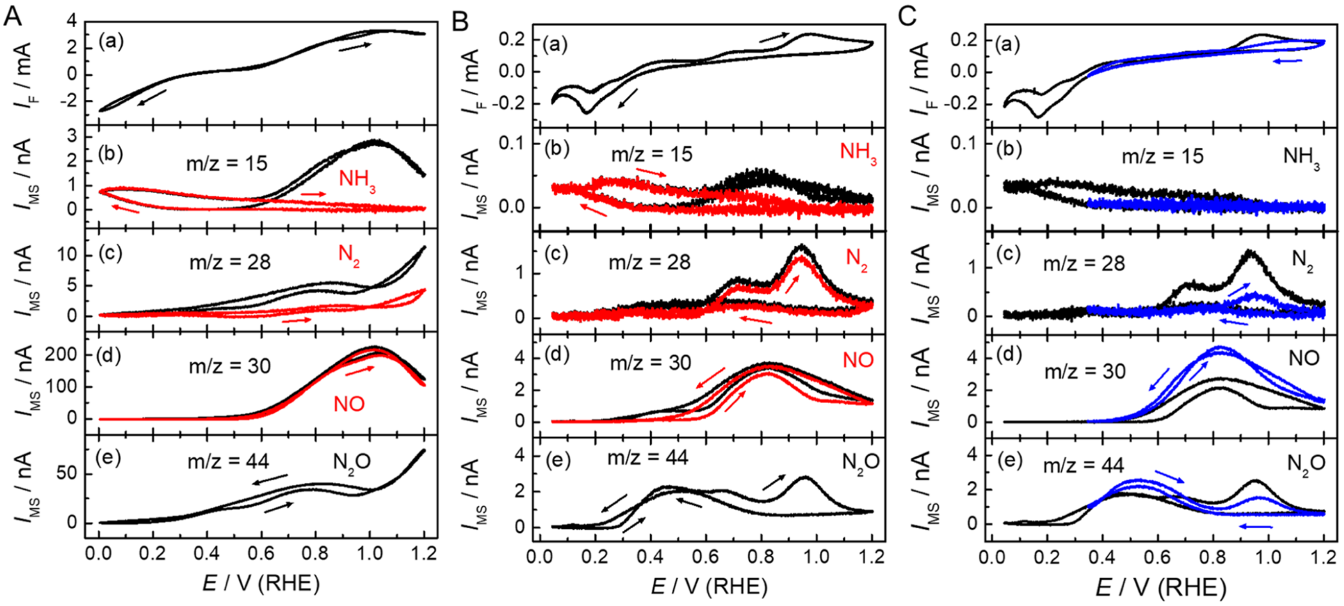

Figure 6. CVs (a) and the corresponding MSCVs of $m/z = 15$ (b), $m/z = 28$ (c), $m/z = 30$ (d), and $m/z = 44$ (e) for NH_2OH oxidation on a Pt film, sputtered on a porous Teflon membrane, in the conventional DEMS cell. Electrolyte: 0.1 M KOH containing 0.1 M NH_2OH (A) or 0.01 M NH_2OH (B, C). Scan rate: 10 mV/s. The red lines in (A, B) indicate the formation of NH_3, N_2, and NO, respectively, after subtracting the contribution from NO and N_2O fragments. (C) Effect(s) of the low potential limit on the oxidation of NH_2OH with a low potential limit of 0.05 (black lines) and 0.35 V (blue lines). In C(b−d), the MS signals represent the contribution only from NH_3, N_2, and NO, respectively.

corresponding MSCVs of $m/z = 15$, 28, 30, and 44 for the oxidation of NH_2OH on Pt in 0.1 M NH_2OH + 0.1 M KOH are presented in Figure 6A. It should be noted that the MS signal of $m/z = 15$ includes the contributions from the NH^+ fragment of NH_3 and the NO^{2+} fragment of NO. The MS signal of $m/z = 28$ (N_2^+) comprised the contributions from both N_2 and N_2O, and the MS signal of $m/z = 30$ (NO^+) included the contributions from both NO and N_2O. The red lines in Figure 6A(b−d) represent the MS signals from NH_3, N_2, and NO respectively, after subtracting contributions from other species. The open circuit potential of NH_2OH was ca. 0.35 V, where the disproportionation of NH_2OH took place,[65−67] as indicated by the formation of N_2O, N_2, and NH_3. As the potential was swept negatively from 0.35 V, the cathodic current increased, while the MS signal at $m/z = 15$ increased, suggesting that NH_2OH was reduced to form NH_3. Upon increasing the potential from 0.35 to 0.6 V, the oxidation current increased slowly, with N_2O as the major product, as indicated by the MS signal of $m/z = 44$. The MS signal of N_2O exhibited two peaks at 0.45 and 0.78 V in the positive-going scan, while a third peak was not fully developed at potentials below 1.2 V. The MS signal of N_2 (red line) also exhibited two peaks at 0.29 and 0.85 V in the positive-going scan, with a non-fully developed third peak at high potentials. At potentials higher than 0.6 V, the oxidation current increased steeply, while a very large MS signal at $m/z = 30$ (red line) was observed, suggesting that NO was the major product for NH_2OH electrooxidation on Pt at potentials of >0.6 V and at high concentrations of NH_2OH. The MS signal of NO (red line) reached a maximum at ca. 1.0 V and then decreased due

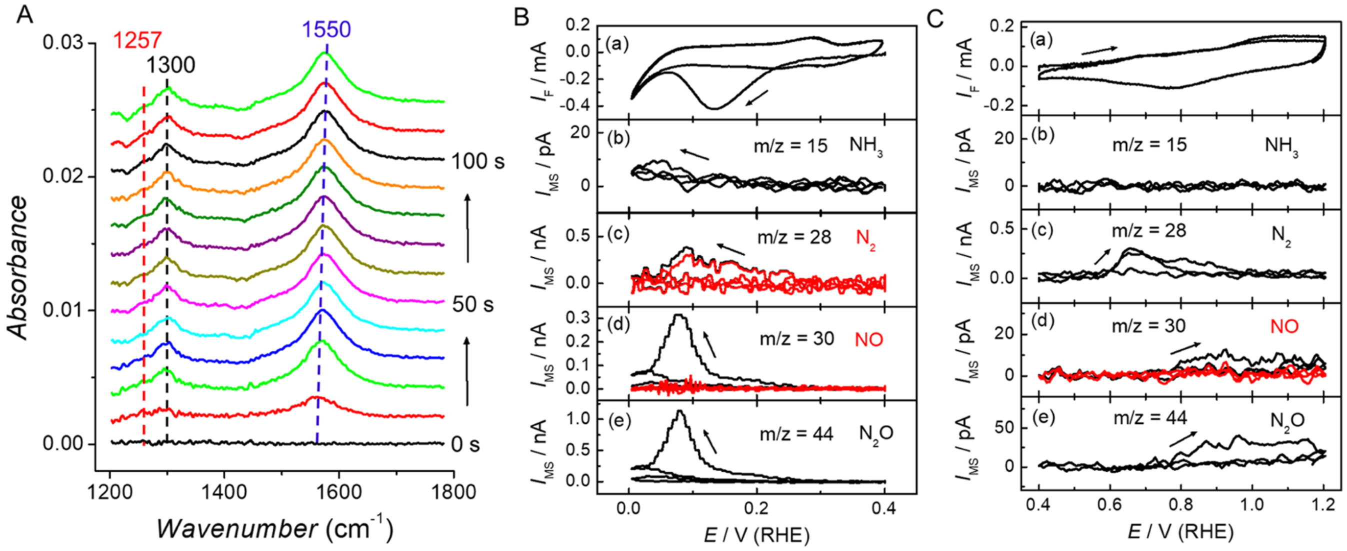

Figure 7. (A) Time-dependent SEIRA spectra for NH_2OH adsorption at 0.4 V in 0.1 M NH_2OH + 0.1 M KOH on a Pt film, chemically deposited on a Si prism, in the dual thin-layer flow cell. The reference spectrum was taken at 0.4 V in 0.1 M KOH. (B, C) CVs (a) and the corresponding MSCVs of m/z = 15, 28, 30, and 44 (b−e) for reductive stripping (B) or oxidative stripping (C) of NH_2OH ad-species from a Pt film, sputtered on a porous Teflon membrane, in the conventional DEMS cell. Scan rate: 50 mV/s.

to the Pt oxide formation and/or its further oxidation to nitrite. The maximum NO signal was parallel to the valley of N_2O and N_2 signals at ca. 1.0 V, suggesting that the formation of NO competed with the formation of N_2 and N_2O. This is likely caused by a lower NH_2OH concentration due to its oxidation to NO.

In 0.01 M NH_2OH, the maximum MS signal of NO negatively shifted to ca. 0.8 V (Figure 6B). The MS signal valley of N_2O, appearing at ca. 0.8 V, also paralleled the maximum MS signal of NO due to their competition for NH_2OH. In the positive-going scan, three N_2O peaks were observed at 0.46, 0.66, and 0.95 V, respectively. In the negative-going scan, two N_2O peaks occurred at 0.52 and 0.12 V, respectively, which are ascribed to the oxidation of NH_2OH and the reduction of NO and NO_2^- that were formed at high potentials, respectively. In 0.01 M NH_2OH, the MS signal at m/z = 28 was mainly ascribed to the fragment from N_2 (red line). The MS signal of N_2 exhibited three peaks at 0.35, 0.71, and 0.94 V, respectively, in the positive-going scan [Figure 6B(c)]. The peak at 0.71 V is ascribed to the oxidation of NH_3 formed in the hydrogen region since this peak disappeared when the low potential limit was higher than 0.35 V [Figure 6C(c), blue lines]. As the low potential limit was increased from 0.05 to 0.35 V, the formation of NO was enhanced at 0.8 V due to less $NH_{x,ad}$ poisoning, while the formation of N_2O and N_2 was suppressed at ca. 0.95 V.

A reduction peak at 0.1−0.2 V in the CV in Figure 6B(a),6C(a) was observed in both negative- and positive-going scan directions. It had no corresponding MS signals at m/z = 15, 28, 30, and 44, and thus can be assigned to the reduction of NO_{ad} to form NH_2OH and $NH_{x,ad}$. $NH_{x,ad}$ is subsequently oxidized to form N_2 at ca. 0.7 V. In Figure 6A(a), the large reduction current at potentials below 0.35 V is mainly attributed to the reduction of NH_2OH to form NH_3 (Figure 6A(b)).

To identify surface ad-species formed during NH_2OH adsorption, time-dependent ATR−SEIRA spectra were recorded (Figure 7A). At 0.4 V, two infrared bands, appearing at 1550 and 1300 cm^{-1}, respectively, are assigned to the ν(NO) of $NO_{ad,B}$[20−22,53] and the δ(H−N−O) and/or δ(H−N−Pt) of NH_2OH_{ad} (Table S1).[68] A weak band, appearing at 1257 cm^{-1}, could be assigned to $NH_{3,ad}$. After NH_2OH adsorption at 0.4 V for 5 min, and subsequent removal of NH_2OH from electrolyte, the potential was scanned between 0 and 0.4 V (Figure 7B) and between 0.4 and 1.2 V (Figure 7C), respectively. Upon reductive stripping of NH_2OH ad-species in the low-potential region, N_2, N_2O, and NH_3 were generated, in contrast to the NH_3 ad-species stripping in which only NH_3 was detected (Figure 2A). Similarly, the chemical reaction between NO and H_2 on Pt catalysts also generated N_2, N_2O, and NH_3.[69] The reduction peak at ca. 0.15 V in Figure 7B(a) was attributed to the reduction of $NO_{ad,B}$ to form NH_2OH and $NH_{x,ad}$. The oxidative stripping of NH_2OH ad-species generated N_2 and N_2O (Figure 7C), exhibiting a much smaller N_2 signal and a much larger N_2O signal than the oxidative stripping of NH_3 ad-species. After negative striping of NH_2OH ad-species, the MS signal of N_2 at ca. 0.7 V significantly increased in the following positive-going scan up to 1.2 V (Figure S9). This suggests that more NH_x ad-species were formed in the negative-going scan due to the reduction of NH_2OH ad-species (mostly $NO_{ad,B}$). N_2 and N_2O were generated in both negative stripping and positive stripping of NH_2OH ad-species. In contrast, N_2 and N_2O could only be generated in the positive stripping of NH_3 ad-species. Infrared spectra revealed that only $NH_{x,ad}$ was formed during NH_3 adsorption at 0.4 V (Figure 4), while NO_{ad}, NH_2OH_{ad}, and even a small amount of $NH_{x,ad}$ were formed during NH_2OH adsorption at 0.4 V (Figure 7A).

2.3.2. Coupled DEMS/ATR−SEIRA Spectroscopic Study of Hydroxylamine Electrooxidation under Well-Defined Flow Conditions.

Simultaneously recorded potentiodynamic DEMS data and SEIRA spectra for NH_2OH electrooxidation on a Pt film, chemically deposited on a Si prism, are presented in Figures S10 and 8A. DEMS data (Figure S10) are similar to those of the Pt film sputtered on a porous Teflon membrane (Figure 6B), except that the Faradaic current density increased due to the enhanced convection in the flow cell, and thus the amounts of formed N_2O and NO also increased. The infrared

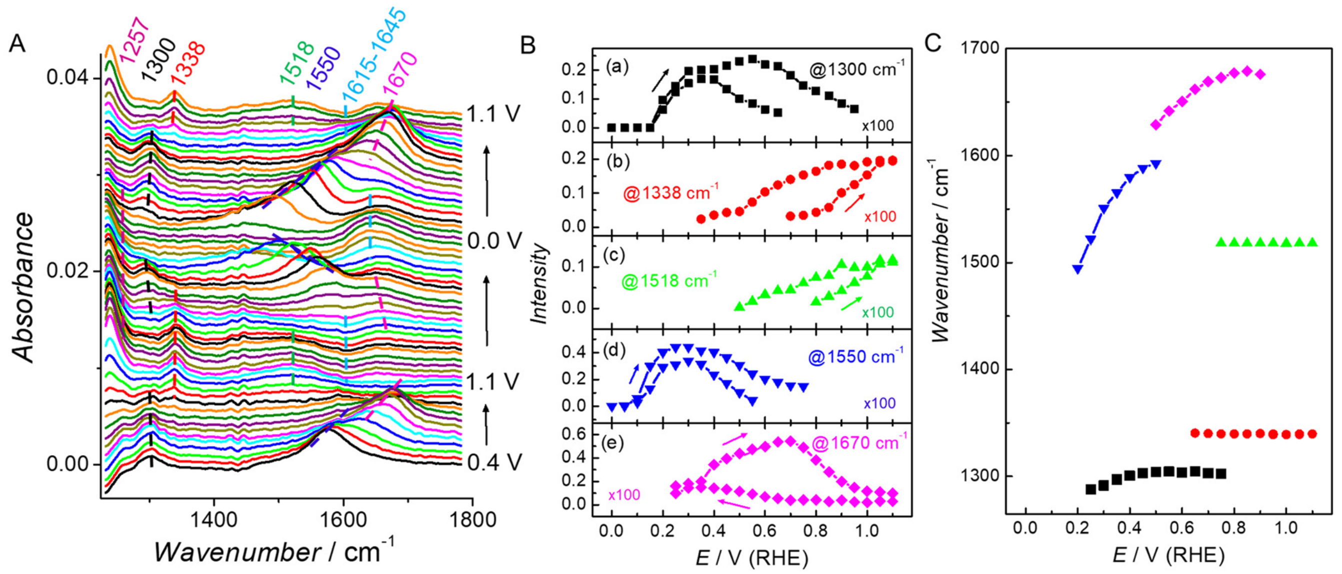

Figure 8. (A) Potential-dependent SEIRA spectra for NH_2OH oxidation/reduction in 0.01 M NH_2OH + 0.1 M KOH on a Pt film, chemically deposited on a Si prism, in the dual thin-layer flow cell. The reference spectrum was taken at 0.4 V in 0.1 M KOH. Scan rate: 5 mV/s. Flow rate: 10 μL/s. (B) Band intensities of NH_2OH_{ad} at 1300 cm^{-1}, $NO_{2,ad}$ at 1338 and 1518 cm^{-1}, $NO_{ad,B}$ at 1550 cm^{-1}, and $NO_{ad,L}$ at 1670 cm^{-1} plotted vs potential. (C) Band wavenumbers plotted vs potential.

band intensities and wavenumbers vs potential are plotted in Figure 8B,8C, respectively. Two infrared bands, appearing at 1550 and 1670 cm^{-1}, can be assigned to the ν(NO) of $NO_{ad,B}$ and linearly bonded NO ($NO_{ad,L}$), respectively (Table S1).[54−57] Their Stark tuning rates were over 500 and 200 cm^{-1}/V in the low-potential region, respectively. These values were much larger than the ca. 30−40 cm^{-1}/V for atop CO and 35−80 cm^{-1} for bridged CO on Pt[41,58,70−72] and also larger than the values observed by other authors for atop and bridged NO on Pt.[73,74] Such a large Stark tuning rate could be attributed to the presence of an unpaired electron in the $2\pi^*$ orbital of NO.[58] NO_{ad} can act as an electron donor or acceptor, which might be strongly dependent on the potential and coverage.[58,75,76] Rodes et al. reported a Stark tuning rate of ca. 50 cm^{-1}/V for the ν(NO) of NO_{ad} on Pt(100) in acidic and neutral solutions.[73] Osawa et al. reported that the ν(NO) band wavenumbers of atop and bridged NO_{ad} on a Pt film with increasing potential exhibited slopes of 73 and 61 cm^{-1}/V, respectively.[74] Weaver et al. observed Stark tuning rates of 62 and 42 cm^{-1}/V for the ν(NO) of a saturated NO adlayer on Pt(111) and Pt(100) surfaces, respectively,[58] and larger Stark tuning rates of 85 and 95 cm^{-1}/V for an NO adlayer at a coverage of 0.3, respectively. A band at 1257 cm^{-1} appeared at low potentials and overlapped with the ν(Si−O−Si), which is assigned to the $\delta_s(NH_3)$ of $NH_{3,ad}$ (Table S1). The band at 1300 cm^{-1} can be assigned to the δ(H−N−O) and/or δ(H−N−Pt) of NH_2OH_{ad}.[68] Two bands at 1338 and 1518 cm^{-1} occurred at potentials higher than 0.8 V in the positive-going scan and in the following reverse scan down to ca. 0.5 V. These two bands appeared when Pt oxides were present on the surface, and thus can be ascribed to the symmetric stretching ν_s(ONO) and asymmetric stretching ν_{as}(ONO) of $NO_{2,ad}$, respectively.[59,60,77−84] The bands at 1615−1645 cm^{-1} are assigned to the bending mode [δ(HOH)] of water adsorbed on Pt.[42] We did not observe the infrared band of N_2O at 2224 cm^{-1},[27] since it is difficult to adsorb on Pt and was swept away after its generation due to the electrolyte flow. The band of $NO_{ad,B}$ at 1550 cm^{-1} appeared at potentials above 0.05 V, and its intensity at first increased with increasing potential and then decreased as the potential went beyond 0.3 V (Figure 8B). The decrease of the $NO_{ad,B}$ band intensity was parallel to an increase in the $NO_{ad,L}$ band intensity. The $NO_{ad,L}$ band intensity reached a maximum at 0.7 V in the positive-going scan, while it occurred at 0.35 V in the negative-going scan. The $NO_{ad,L}$ band intensity was much lower in the negative-going scan than that in the positive-going scan, likely due to sluggish $NO_{2,ad}$ and Pt oxide reductions. As the potential went up from 0.8 V, the intensities of $NO_{2,ad}$ bands at 1338 and 1518 cm^{-1} increased with increasing potential. Like oxygen adsorption, the NO_2 adsorption was also irreversible and the bands disappeared at potentials below 0.5 V in the reverse scan.

The MS signal of NO in both positive-going and negative-going scans exhibited very similar profiles, intensities, and peak potentials. In contrast, the $NO_{ad,L}$ band intensity in the negative-going scan was much smaller than in the positive-going scan. This suggests that NH_2OH is oxidized to NO likely through a weakly adsorbed NO rather than $NO_{ad,L}$. The MS signal of NO onset at 0.5−0.6 V, where a large amount of OH_{ad} is present.[42] The MS signal peak of NO was positively shifted as the concentration of NH_2OH increased, similar to the electrooxidation of methanol.[85] Therefore, NO was likely formed through the reaction between NH_2OH_{ad} and OH_{ad}, as shown below:

$$NH_2OH_{ad} + 3OH_{ad} \rightarrow NO + 3H_2O \qquad (11)$$

At low potentials (in the hydrogen region), NH_3 was formed through a reaction between H_{ad} and NH_2OH_{ad} as shown below

$$NH_2OH_{ad} + 2H_{ad} \rightarrow NH_3 + H_2O \qquad (12)$$

Meanwhile, N_2O and N_2 were generated at potentials below 0.3 V in the negative-going scan through the following reactions, respectively:[69,86]

$$NO_{ad} + H_{ad} \rightarrow HNO_{ad} \qquad (13)$$

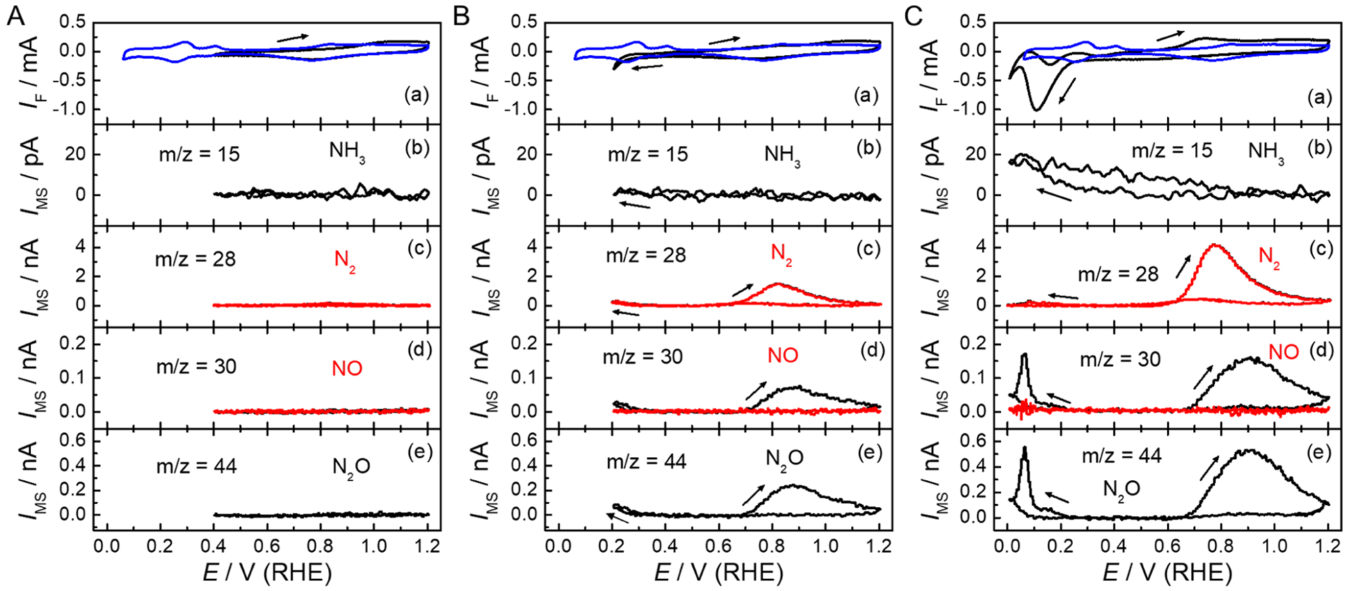

Figure 9. CVs (a) and the corresponding MSCVs of m/z = 15 (b), m/z = 28 (c), m/z = 30 (d), and m/z = 44 (e) for NO_2^- reduction at a Pt film, sputtered on a porous Teflon membrane, in the conventional DEMS cell with the low potential limit of 0.4 (A), 0.2 (B), and 0 V (C). Electrolyte: 0.01 M $NaNO_2$ + 0.1 M KOH. Scan rate: 50 mV/s. The blue lines in (a) present the CVs in 0.1 M KOH. The red lines in (c, d) indicate the MS signals of N_2 and NO, respectively.

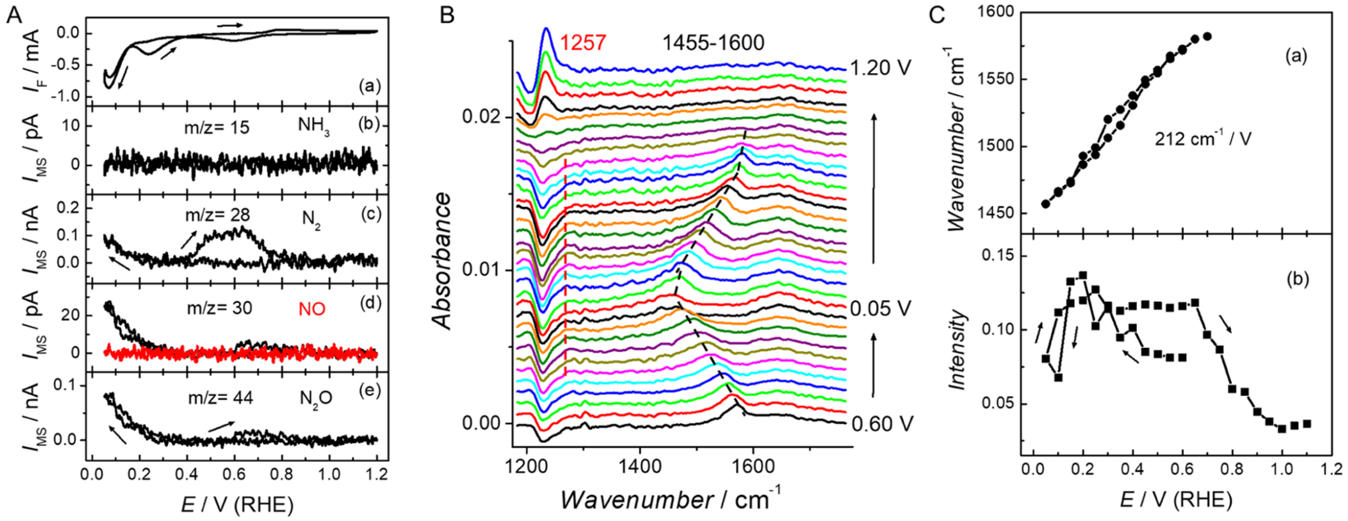

Figure 10. (A) CV (a) and the corresponding MSCVs of m/z = 15 (b), m/z = 28 (c), m/z = 30 (d), and m/z = 44 (e) for NO_2^- reduction on a Pt film, chemically deposited on a Si prism, in the dual thin-layer flow cell. Electrolyte: 0.01 M $NaNO_2$ + 0.1 M KOH. Scan rate: 5 mV/s. Flow rate: 10 μL/s. (B) Potential-dependent SEIRA spectra for NO_2^- reduction on the Pt film. The reference spectrum was taken at 0.6 V in 0.1 M KOH. (C) Wavenumber (a) and integrated band intensity at 1400−1600 cm^{-1} (b) plotted vs potential.

$$2HNO_{ad} \rightarrow H_2N_2O_{2,ad} \tag{14}$$

$$H_2N_2O_{2,ad} \rightarrow N_2O + H_2O \tag{15}$$

$$H_2N_2O_{2,ad} + 2H_{ad} \rightarrow N_2 + 2H_2O \tag{16}$$

At potentials >0.3 V, N_2O was likely formed through the following reactions:[27,87,88]

$$NH_2OH_{ad} + 2OH_{ad} \rightarrow HNO_{ad} + 2H_2O \tag{17}$$

$$2HNO_{ad} \rightarrow N_2O + H_2O \tag{18}$$

while N_2 was likely formed through the following reaction:

$$NH_2OH_{ad} + HNO_{ad} \rightarrow N_2 + 2H_2O \tag{19}$$

At potential around 0.8 V (Figure 6B,6C) or 1 V (Figure 6A), the formation of NO suppressed the formation of N_2O and N_2 due to their competition for NH_2OH. At even higher potentials (>0.95 V, Figure 6B), the MS signals of N_2 and N_2O decreased due to the further oxidation of Pt and the formation of $NO_{2,ad}$.

2.4. Nitrite Electroreduction on Pt. *2.4.1. DEMS Study of NO_2^- Electroreduction under Stationary Electrolyte Condition.* As mentioned above, NO_2^- was formed during the AOR on Pt at high potentials, and it can also be reduced back to form NH_3. The study of NO_2^- electroreduction on Pt could lead to a further understanding of the AOR mechanism. Thus, we also investigated NO_2^- electroreduction on Pt. First, we studied how the low potential limit affected the products of

NO_2^- reduction, and the DEMS data are presented in Figure 9. When the low potential limit was above 0.4 V, the MS signals of N_2O, N_2, and NH_3 were not observed. In contrast, as the low potential limit went into the hydrogen region, N_2O, N_2, and NH_3 were formed. In the subsequent positive-going scan, N_2 and N_2O were formed at potentials higher than 0.6 V, and were ascribed to the oxidation of NH_3 and NH_2OH, respectively, formed in the hydrogen region in the negative-going scan.

In order to verify that the formation of N_2O could be attributed to the oxidation of NH_2OH that formed in the hydrogen region, rather than to the coupling between NO and NH_x ad-species formed during nitrite reduction, we performed the nitrite reduction and AOR simultaneously in an 0.1 M KOH electrolyte containing both 0.01 M NO_2^- and 0.1 M NH_3 (Figure S11). Compared to the electrolyte containing only NH_3, the formation of N_2 was suppressed in the electrolyte containing both NH_3 and $NaNO_2$ due to the blockage by NO_{ad}. When the low potential limit was set above 0.4 V, the N_2O formation was not affected by the presence of $NaNO_2$ (Figure S11A). In contrast, as the low potential was set below 0.4 V, the N_2O formation increased (Figure S11B). Thus, the formation of N_2O at high potentials is ascribed to the oxidation of NH_2OH that was formed via the reduction of nitrite in the hydrogen region.

2.4.2. Coupled DEMS/ATR-SEIRA Spectroscopic Study of NO_2^- Electroreduction under Well-Defined Electrolyte Flow Conditions. Simultaneously recorded DEMS data and SEIRA spectra for NO_2^- reduction on a Pt film, chemically deposited on a Si prism, in the flow cell are presented in Figure 10. The DEMS data also showed that the formation of N_2O and N_2 occurred at potentials below 0.3 V, as well as at high potentials in the following positive-going scan, similar to those of the Pt film, sputtered on a porous Teflon membrane (Figure 9). NH_3 was difficult to observe due to its low volatility and small collection efficiency of the flow cell. An infrared band observed at 1455−1600 cm^{-1}, is assigned to the $\nu(NO)$ of $NO_{ad,B}$ with a Sark tuning rate of 212 cm^{-1}/V [Figure 10C(a)]. The band for $NO_{ad,L}$ was not observed due to a lower NO coverage (Figure S5), unlike the case of NH_2OH oxidation. A weak band at 1257 cm^{-1}, assigned to the $\delta(NH_3)$ of $NH_{3,ad}$, occurred in the hydrogen region and disappeared at potentials higher than 0.6 V since it is oxidized to form N_2. The band for NH_2OH_{ad} was too weak to be observed. The integrated band intensity at 1400−1600 cm^{-1} is plotted vs potential in Figure 10C(b). At an initial potential of 0.6 V, the band of $NO_{ad,B}$ appeared due to NO_2^- reduction. As the potential went down from 0.6 V, its intensity increased first and then decreased at potentials below 0.2 V since it was reductively removed [Figure 10A(c,e)]. In the subsequent positive-going scan, its intensity increased again first and reached a plateau at potentials between 0.3 and 0.65 V. With further increasing potential, its intensity decreased gradually due to its oxidation back to NO_2^-.

The simultaneously recorded DEMS data and SEIRA spectra for NO_2^- adsorbate stripping from a Pt film, chemically deposited on a Si prism, are presented in Figure S12. In the negative-going scan, N_2O, N_2, and NH_3 were formed in the low potential region, similar to the bulk reduction of NO_2^-. The DEMS data for NO_2^- adsorbate stripping from a Pt film, sputtered on a porous Teflon membrane, also exhibited a similar behavior (Figure S5). SEIRA spectra showed that $NO_{ad,B}$ was formed on the Pt surface, and most of it was reductively desorbed to form N_2O, N_2, and NH_3 in the negative-going scan, while a portion of $NO_{ad,B}$ was reduced to form $NH_{x,ad}$, as indicated by the band at 1257 cm^{-1} in Figure S12B.

2.5. New Insights into the Mechanism of the AOR.

SEIRA spectra suggested that $NH_{3,ad}$ and $NH_{2,ad}$ species were formed at potentials around 0.4 V, where N_2 was not detected by DEMS. Furthermore, during the AOR, the N_2 formation rate was parallel to the band intensity of NH_{ad}. This suggests that NH_{ad} is the likely precursor for N−N coupling to form N_2 rather than $NH_{2,ad}$ during the AOR on Pt. At more positive potentials, NH_{ad} was further oxidized to N_2O and NO, likely through HNO_{ad}. Two HNO_{ad} could couple to form N_2O or could be further oxidized to NO. However, the band of HNO_{ad} could not be identified by using SEIRA spectroscopy likely due to its low coverage and/or its overlap with the $NO_{ad,B}$ band.

The electrooxidation of NH_2OH is much more facile than ammonia due to the presence of the OH group. This is similar to the trend for hydrocarbons in which methanol and ethanol are more easily electrooxidized than methane and ethane. In both cases, the more highly oxygenated, the more easily oxidized the molecules are.

NH_2OH electrooxidation generated a large amount of N_2O at potentials >0.2 V, while the AOR generated N_2O at potentials >0.75 V. These results suggest that N- and O-containing species must be involved in the N−N coupling to form N_2O. These O- and N-containing species must also contain H atoms since no N_2O was formed for NO_2^- electroreduction above the hydrogen region. Therefore, the O-, N-, and H-containing ad-species are likely HNO_{ad} or NO_{ad} and $NH_{x,ad}$ co-adsorbates. N_2O is formed through two HNO_{ad} couplings rather than NO_{ad} and $NH_{x,ad}$ coupling, as mentioned above.[89]

The Stark tuning rates for $NO_{ad,L}$ and $NO_{ad,B}$ were higher than 200 and 500 cm^{-1}/V, respectively, which are much higher than previously reported values.[73,74,90,91] This suggests that besides the Stark effect, $NO_{ad,L}$ and $NO_{ad,B}$ might change their chemical state from HNO/NO^- to NO and further to NO^+ with increasing potential.[54−57,92] In addition, NO_{ad} might gradually change its adsorption site with potential, resulting in the large Stark tuning rate.[58]

In ultrahigh vacuum (UHV), Pt was found to be the most active among pure metal catalysts for the catalytic oxidation of NH_3 with O_2. The reaction between NH_3 and O_2 on Pt single crystals and nanoparticles generated N_2, N_2O, and NO, which were formed successively at low, medium, and high temperatures, respectively.[52,93−95] In other words, the onset temperature of the oxidation products increased in the sequence: $N_2 < N_2O <$ NO. Similarly, the onset potentials of N_2, N_2O, and NO for the AOR on Pt increased in the same sequence. The selectivity of extensive oxidation products such as N_2O and NO also increased with the increasing partial pressure ratio of O_2/NH_3 for the catalytic oxidation of NH_3 with O_2 on Pt surfaces.[95] This is the same sequence as the AOR on Pt electrodes in which the yield of extensive oxidation products increased with increasing potential.

In the case of catalytic oxidation of NH_3 with O_2, it was postulated that N_2 was formed through the coupling reaction between two NH_x ad-species and then further dehydrogenation of $N_2H_{2x,ad}$, while N_2O was generated through the dimerization of HNO_{ad}.[43−48,89] NO was proposed to be formed through further oxidation of HNO_{ad} with adsorbed O.[52,95,96]

Due to the above-mentioned similarity between the AOR and the oxidation of NH_3 with O_2, similar intermediates and mechanism can be expected. Combined with our spectroscopic observations, the alkaline AOR mechanism on Pt can be then described by the following scheme/sequence:

$$NH_3 \rightarrow NH_{3,ad} \tag{20}$$

$$NH_{3,ad} + OH^- \rightarrow NH_{2,ad} + H_2O + e^- \tag{21}$$

$$NH_{2,ad} + OH^- \rightarrow NH_{ad} + H_2O + e^- \tag{22}$$

$$2NH_{ad} \rightarrow N_2H_{2,ad} \tag{23}$$

$$N_2H_{2,ad} + 2OH^- \rightarrow N_2 + 2H_2O + 2e^- \tag{24}$$

$$NH_{ad} + 2OH^- \rightarrow HNO_{ad} + H_2O + 2e^- \tag{25}$$

$$2HNO_{ad} \rightarrow N_2O + H_2O \tag{26}$$

$$HNO_{ad} + OH^- \rightarrow NO + H_2O + e^- \tag{27}$$

$$NH_{ad} + OH^- \rightarrow N_{ad} + H_2O + e^- \tag{28}$$

Our coupled DEMS and ATR−SEIRA spectra provided clear evidence that NH ad-species are the precursors for the N−N coupling to form N_2 rather than NH_2 ad-species, while HNO ad-species are the precursors for the formation of N_2O rather than NH_x and NO co-adsorbates. In addition, NH_2OH is less likely the intermediate for the AOR, since no infrared bands of NH_2OH were observed. The infrared band of NH_{ad} could be observed at very high potentials, such as 1.2 V, suggesting that the oxidation of NH_{ad} to form N_2 was slow at high potentials. As mentioned above, the electrooxidation of hydrazine exhibits very fast kinetics. Once the NH−NH is formed, it would be immediately oxidized to N_2 and thus its infrared band could not be observed. The presence of NH_{ad} on Pt at high potentials suggests that the NH−NH coupling became the rds for the AOR at high potentials.

Assuming that the adsorption of NH_x species obeys a Langmuir isotherm due to their low coverages and that the first dehydrogenation step (eq 21) is the rds, the reaction rate would be given by $r_1 = k_1\, \theta_{NH_3} \exp(\alpha F\eta/RT)$ and thus the Tafel slope would be 118 mV/dec with $\alpha = 0.5$.[1] If the second dehydrogenation step (eq 22) is the rds and the first dehydrogenation step (eq 21) is in equilibrium, the reaction rate $r_2 = k_2 K_1 \theta_{NH_3} \exp[(1 + \alpha)F\eta/RT]$, and thus the Tafel slope would be 39 mV/dec with $\alpha = 0.5$.[1] Here, η is the overpotential, α is the electron transfer coefficient, F is Faraday's constant, θ_{NH_3} is the coverage of NH_3, K_1 is the equilibrium constant of eq 21, and k_1 and k_2 are the rate constants for eqs 21 and 22, respectively. While the above analysis assumed that the coverage of NH_3 was (for simplicity) independent of potential, it is likely that the value is potential-dependent. Thus, the Tafel analysis is less rigorous. The observed Tafel slope for the AOR on the Pt films in 0.1 M KOH + 0.1 M NH_3 at the initial N_2 formation potentials (around 0.6 V) was ca. 100−110 mV/dec (Figure S13), suggesting that the first dehydrogenation step is likely the rds at the initial N_2 formation potentials. The observed Tafel slope is much larger than the values observed in 1 M KOH (30−40 mV/dec).[1,16,97] This could be caused by the OH^- concentration or pH difference. Li et al. reported that the AOR current increased with increasing concentration of KOH.[97] Increasing OH^- concentration might enhance the first dehydrogenation process (eq 21), shifting the rds from the first to the second dehydrogenation step, and thus resulting in a decrease in the Tafel slope from 100 to 30 mV/dec.

The Tafel slope for the AOR has also been reported to vary on different single-crystal Pt surfaces.[12] The AOR predominantly occurred on Pt(100) facets, with stepped Pt(100) surfaces exhibiting lower kinetics. As a result, the Tafel slope changed from 28 mV/dec on Pt(100) to 94 mV/dec on Pt(311). On Pt(210), the Tafel slope was 40 mV/dec at low potentials and 128 mV/dec at high potentials, respectively.[12] This indicates that the rds can vary with Pt facets and potentials. For our Pt films, the H adsorption peak of Pt(100) facets was completely suppressed by NH_3 ad-species (Figure S4), suggesting that Pt(100) facets adsorb $NH_{x,ad}$ more strongly than the other facets.

With increasing potential, some water molecules were gradually replaced by OH^- anions in the double layer (Figures 3B and S8), and thus the pH increased at/near the electrode surface. This further favored the ammonia dehydrogenation. In eqs 21−28, hydroxide anion could be partially oxidized to form hydroxyl ad-species and even oxides. To elucidate the effect of hydroxyl ad-species on the AOR, we also studied the AOR on a Ru-modified Pt film (Pt/Ru). It is well known that hydroxyl ad-species can be formed on Ru at lower potentials than on Pt. We found that the onset potential of AOR on Pt/Ru was negatively shifted, relative to pure Pt, but the peak current significantly decreased (Figure S14). This is similar to methanol electrooxidation on Pt/Ru.[98] The AOR enhancement by Ru modification is attributed to the enhanced dehydrogenation by adsorbed hydroxyl and/or increased adsorption energy,[10] while the suppression at high potentials is due to the blockage by oxides.

3. CONCLUSIONS

The alkaline AOR on Pt has been studied using coupled DEMS and ATR−SEIRA spectroscopy. NH_2NH_2 electrooxidation, NH_2OH electrooxidation/reduction, and NO_2^- electroreduction on Pt have also been studied to further elucidate the AOR mechanism. N_2, N_2O, and NO were detected by using DEMS as the products of the AOR on Pt, while $NH_{3,ad}$, $NH_{2,ad}$, NH_{ad}, NO_{ad}, and $NO_{2,ad}$ were identified as surface ad-species by using ATR−SEIRA spectroscopy. As the potential increased, $NH_{3,ad}$ was gradually dehydrogenated to form $NH_{2,ad}$ and then NH_{ad} on Pt. The maximum intensities of $NH_{3,ad}$, $NH_{2,ad}$, and NH_{ad} appeared at ca. 0.35, 0.5, and 0.7 V, respectively. The onset potentials of N_2, N_2O, and NO were ca. 0.5, 0.75, and 1.0 V, respectively. With increasing potentials, the selectivity of the extensive oxidation products increased.

NH_2NH_2 electrooxidation on Pt to form N_2 onset at ca. 0.1 V and its kinetics are very fast. In contrast, the AOR formed N_2 onset at around 0.5 V, where a maximum coverage of $NH_{2,ad}$ was observed. Therefore, the formation of N_2, for the AOR on Pt, is unlikely through the dimerization of $NH_{2,ad}$ to form $NH_2NH_{2,ad}$ as intermediate, which was not observed with SEIRA spectroscopy in this work. The MS signal profile of N_2 for potentiodynamic AOR on Pt was parallel to the plot of band intensity of NH_{ad} vs potential, suggesting that NH_{ad} is the precursor for the N−N coupling to form N_2.

NH_2OH electrooxidation on Pt generated large amounts of N_2O and NO, and also small amounts of NH_3 and N_2, while $NO_{ad,B}$, $NO_{ad,L}$, $NH_{3,ad}$, NH_2OH_{ad}, and $NO_{2,ad}$ were identified as adsorbed species on Pt surfaces. The AOR on Pt is less likely through NH_2OH as an intermediate since the electrooxidation of NH_2OH mainly generates N_2O and NO rather than N_2.

N_2, N_2O, NH_2OH, and NH_3 were formed during the electroreduction of NO_2^- in the hydrogen region, while $NO_{ad,B}$ and $NH_{x,ad}$ were identified as ad-species. $NO_{ad,B}$ can be oxidized back to NO_2^- at potentials >0.8 V or reduced to form N_2, N_2O, NH_2OH, and NH_3 in the hydrogen region.

The coupled DEMS and ATR−SEIRA spectroscopic observations brought light to the alkaline AOR mechanism, that was until now, not yet completely understood. To facilitate the AOR to form N_2, we need to find electrocatalysts that can enhance the dehydrogenation of NH_3 to form NH_{ad} and also can facilitate the dimerization of NH_{ad}. These new insights are crucial for the development of future highly active AOR catalysts.

■ ASSOCIATED CONTENT

Supporting Information

The Supporting Information is available free of charge at https://pubs.acs.org/doi/10.1021/jacs.4c02621.

Experimental details; additional DEMS data and SEIRA spectra; and the table of infrared band assignment (PDF)

■ AUTHOR INFORMATION

Corresponding Author

Héctor D. Abruña − *Department of Chemistry and Chemical Biology, Baker Laboratory, Cornell University, Ithaca, New York 14853-1301, United States;* orcid.org/0000-0002-3948-356X; Email: hda1@cornell.edu

Authors

Hongsen Wang − *Department of Chemistry and Chemical Biology, Baker Laboratory, Cornell University, Ithaca, New York 14853-1301, United States;* orcid.org/0000-0001-7926-2895

Dario R. Dekel − *Department of Chemistry and Chemical Biology, Baker Laboratory, Cornell University, Ithaca, New York 14853-1301, United States; The Wolfson Department of Chemical Engineering and The Nancy & Stephen Grand Technion Energy Program (GTEP), Technion—Israel Institute of Technology, Haifa 3200003, Israel;* orcid.org/0000-0002-8610-0808

Complete contact information is available at: https://pubs.acs.org/10.1021/jacs.4c02621

Notes

The authors declare no competing financial interest.

■ ACKNOWLEDGMENTS

This material is based upon work supported by the Air Force Office of Scientific Research under the MURI: Molecular Level Studies of Solid−Liquid Interfaces in Electrochemical Processes award number FA9550-18-1-0420. This work made use of the Cornell Center for Materials Research Shared Facilities which are supported through the NSF MRSEC program (DMR-1719875). D.R.D.'s contribution was supported by the Israeli Science Foundation, grant number 169/22, and the Technion Center for Security Science & Technology (CSST), grant no. 2070769.

■ REFERENCES

(1) Oswin, H. G.; Salomon, M. The Anodic Oxidation of Ammonia at Platinum Black Electrodes in Aqueous KOH Electrolyte. *Can. J. Chem.* **1963**, *41*, 1686−1694.

(2) Gerischer, H.; Mauerer, A. Untersuchungen Zur Anodischen Oxidation von Ammoniak an Platin-Electroden. *J. Electroanal. Chem. Interfacial Electrochem.* **1970**, *25*, 421−433.

(3) Rosca, V.; Duca, M.; de Groot, M. T.; Koper, M. T. M. Nitrogen Cycle Electrocatalysis. *Chem. Rev.* **2009**, *109*, 2209−2244.

(4) Siddharth, K.; Chan, Y.; Wang, L.; Shao, M. Ammonia Electrooxidation Reaction: Recent Development in Mechanistic Understanding and Electrocatalyst Design. *Curr. Opin. Electrochem.* **2018**, *9*, 151−157.

(5) Wasmus, S.; Vasini, E. J.; Krausa, M.; Mishima, H. T.; Vielstich, W. DEMS-Cyclic Voltammetry Investigation of the Electrochemistry of Nitrogen Compounds in 0.5 M Potassium Hydroxide. *Electrochim. Acta* **1994**, *39*, 23−31.

(6) Katsounaros, I.; Figueiredo, M. C.; Calle-Vallejo, F.; Li, H.; Gewirth, A. A.; Markovic, N. M.; Koper, M. T. M. On the Mechnism of the Electrochemical Conversion of Ammonia to Dinitrogen on Pt(100) in Alkaline Environment. *J. Catal.* **2018**, *359*, 82−91.

(7) Yang, K.; Liu, J.; Yang, B. Mechnism and Active Species in NH_3 Dehydrogenation under an Electrochemical Environment: An Ab Initio Molecular Dynamics Study. *ACS Catal.* **2021**, *11*, 4310−4318.

(8) Yang, K.; Liu, J.; Yang, B. Electrocatalytic Oxidation of Ammonia on Pt: Mechanistic Insights into the Formation of N_2 in Alkaline Media. *J. Catal.* **2022**, *405*, 626−633.

(9) Pillai, H. S.; Xin, H. New Insights into Electrochemical Ammonia Oxidation on Pt(100) from First Principles. *Ind. Eng. Chem. Res.* **2019**, *58*, 10819−10828.

(10) de Vooys, A. C. A.; Koper, M. T. M.; van Santen, R. A.; van Veen, J. A. R. The Role of Adsorbates in the Electrochemical Oxidation of Ammonia on Noble and Transition Metal Electrodes. *J. Electroanal. Chem.* **2001**, *506*, 127−137.

(11) Vidal-Iglesias, F. J.; Solla-Gullon, J.; Feliu, J. M.; Baltruschat, H.; Aldaz, A. DEMS Study of Ammonia Oxidation on Platinum Basal Planes. *J. Electroanal. Chem.* **2006**, *588*, 331−338.

(12) Vidal-Iglesias, F. J.; Solla-Gullon, J.; Montiel, V.; Feliu, J. M.; Aldaz, A. Ammonia Selective Oxidation on Pt(100) Sites in an Alkaline Medium. *J. Phys. Chem. B* **2005**, *109*, 12914−12919.

(13) Vidal-Iglesias, F. J.; Garcia-Araez, N.; Montiel, V.; Feliu, J. M.; Aldaz, A. Selective Electrocatalysis of Ammonia Oxidation on Pt(100) Sites in Alkaline Medium. *Electrochem. Commun.* **2003**, *5*, 22−26.

(14) Vidal-Iglesias, F. J.; Solla-Gullon, J.; Rodriguez, P.; Herrero, E.; Montiel, V.; Feliu, J. M.; Aldaz, A. Shape-Dependent Electrocatalysis: Ammonia Oxidation on Platinum Nanoparticles with Preferential (100) Surfaces. *Electrochem. Commun.* **2004**, *6*, 1080−1084.

(15) Herron, J. A.; Ferrin, P.; Mavrikakis, M. Electrocatalytic Oxidation of Ammonia on Transition-Metal Surfaces: A First-Principles Study. *J. Phys. Chem. C* **2015**, *119*, 14692−14701.

(16) Rosca, V.; Koper, M. T. M. Electrocatalytic Oxidation of Ammonia on Pt(111) and Pt(100) Surfaces. *Phys. Chem. Chem. Phys.* **2006**, *8*, 2513−2524.

(17) Skachkov, D.; Rao, C. V.; Ishikawa, Y. Combined First-Principles Molecular Dynamics/Density Functional Theory Study of Ammonia Electrooxidation on Pt(100) Electrode. *J. Phys. Chem. C* **2013**, *117*, 25451−25466.

(18) Vidal-Iglesias, F. J.; Solla-Gullon, J.; Perez, J. M.; Aldaz, A. Evidence by SERS of Azide Anion Participation in Ammonia Electrooxidation in Alkaline Medium on Nanostructured Pt Electrodes. *Electrochem. Commun.* **2006**, *8*, 102−106.

(19) de Vooys, A. C. A.; Mrozek, M. F.; Koper, M. T. M.; van Santen, R. A.; van Veen, J. A. R.; Weaver, M. J. The Nature of Chemisorbates Formed from Ammonia on Gold and Palladium Electrodes as Discerned from Surface-Enhanced Raman Spectroscopy. *Electrochem. Commun.* **2001**, *3*, 293−298.

(20) Matsui, T.; Suzuki, S.; Katayama, Y.; Yamauchi, K.; Okanishi, T.; Muroyama, H.; Eguchi, K. In Situ Attenuated Total Reflection Infrared Spectroscopy on Electrochemical Ammonia Oxidation over

Pt Electrode in Alkaline Aqueous Solution. *Langmuir* **2015**, *31*, 11717−11723.

(21) Katayama, Y.; Okanishi, T.; Muroyama, H.; Matsui, T.; Eguchi, K. Enhanced Supply of Hydroxyl Species in CeO_2-Modified Platinum Catalyst Studied by In Situ ATR-FTIR Spectroscopy. *ACS Catal.* **2016**, *6*, 2026−2034.

(22) Katayama, Y.; Okanishi, T.; Muroyama, H.; Matsui, T.; Eguchi, K. Enhancement of Ammonia Oxidation Activity over Y_2O_3-Modified Platinum Surface: Promotion of $NH_{2,ad}$ Dimerization Process. *J. Catal.* **2016**, *344*, 496−506.

(23) Wei, R.-L.; Liu, Y.; Chen, Z.; Jia, W.-S.; Yang, Y.-Y.; Cai, W.-B. Ammonia Oxidation on Iridium Electrode in Alkaline Media: An In Situ ATR-SEIRAS Study. *J. Electroanal. Chem.* **2021**, *896*, No. 115254.

(24) Endo, K.; Katayama, Y.; Miura, T. A Rotating Disk Electrode Study on the Ammonia Oxidation. *Electrochim. Acta* **2005**, *50*, 2181−2185.

(25) Chen, J. G.; Crooks, R. M.; Seefeldt, L. C.; Bren, K. L.; Bullock, R. M.; Darensbourg, M. Y.; Holland, P. L.; Hoffman, B.; Janik, M. J.; Jones, A. K.; Kanatzidis, M. G.; King, P.; Lancaster, K. M.; Lymar, S. V.; Pfromm, P.; Schneider, W. F.; Schrock, R. R. Beyond Fossil Fuel-Driven Nitrogen Transformations. *Science* **2018**, *360*, No. eaar6611.

(26) Duca, M.; Figueiredo, M. C.; Climent, C.; Rodriguez, P.; Feliu, J. M.; Koper, M. T. M. Selective Catalytic Reduction at Quasi-Perfect Pt(100) Domains: A Universal Low-Temperature Pathway from Nitrite to N_2. *J. Am. Chem. Soc.* **2011**, *133*, 10928−10939.

(27) Jebaraj, A. J. J.; de Godoi, D. R. M.; Scherson, D. The Oxidation of Hydroxylamine on Pt- and Pd-Modified Au Electrodes in Aqueous Electrolytes: Electrochemical and In Situ Spectroscopic Studies. *Catal. Today* **2013**, *202*, 44−49.

(28) Miao, R.; Compton, R. G. Mechanism of Hydrazine Oxidation at Palladium Electrodes: Long-Lived Radical Dication Formation. *Electrochim. Acta* **2021**, *388*, No. 138655.

(29) Rosca, V.; Koper, M. T. M. Electrocatalytic Oxidation of Hydrazine on Platinum Electrodes in Alkaline Solutions. *Electrochim. Acta* **2008**, *53*, 5199−5205.

(30) Rosca, V.; Beltramo, G. L.; Koper, M. T. M. Hydroxylamine Electrochemistry at Polycrystalline Platinum in Acidic Media: A Voltammetric, DEMS and FTIR Study. *J. Electroanal. Chem.* **2004**, *566*, 53−62.

(31) Karabinas, P.; Wolter, O.; Heitbaum, J. Mechanistic Studies with Mass Spectroscopic Cyclic Voltammetry: Anodic Oxidation of Hydroxylamine on Pt. *Ber. Bunsenges. Phys. Chem.* **1984**, *88*, 1191−1196.

(32) Rosca, V.; Beltramo, G. L.; Koper, M. T. M. Hydroxylamine Electrochemistry at Low-Index Single-Crystal Platinum Electrodes in Acidic Media. *J. Phys. Chem. B* **2004**, *108*, 8294−8304.

(33) Pozniak, B.; Treufeld, I.; Scherson, D. Hydroxylamine Oxidation on Polycrystalline Gold Electrodes in Aqueous Electrolytes: Quantitative On-Line Mass Spectrometry under Forced Convection. *ChemPhysChem* **2019**, *20*, 3128−3133.

(34) Duca, M.; Kavvadia, V.; Rodriguez, P.; Lai, S. C. S.; Hoogenboom, T.; Koper, M. T. M. New Insights into the Mechanism of Nitrite Reduction on a Platinum Electrode. *J. Electroanal. Chem.* **2010**, *649*, 59−68.

(35) Duca, M.; van der Klugt, B.; Hasnat, M. A.; Machida, M.; Koper, M. T. M. Electrocatalytic Reduction of Nitrite on a Polycrystalline Rhodium Electrode. *J. Catal.* **2010**, *275*, 61−69.

(36) Bae, I. T.; Barbour, R. L.; Scherson, D. A. In Situ Fourier Transform Infrared Spectroscopic Studies of Nitrite Reduction on Platinum Electrodes in Perchloric Acid. *Anal. Chem.* **1997**, *69*, 249−252.

(37) Burke, L. D.; O'Dwyer, K. J. Oxidationof Some Reactive Small Molecules on Copper and Platinum in Solutions of High pH. *Electrochim. Acta* **1991**, *36*, 1937−1945.

(38) Ko, B. H.; Hasa, B.; Shin, H.; Zhao, Y.; Jiao, F. Electrochemical Reduction of Gaseous Nitrogen Oxides on Transition Metals at Ambient Conditions. *J. Am. Chem. Soc.* **2022**, *144*, 1258−1266.

(39) Rosca, V.; Beltramo, G. L.; Koper, M. T. M. Reduction of NO Adlayers on Pt(110) and Pt(111) in Acidic Media: Evidence for Adsorption Site-Specific Reduction. *Langmuir* **2005**, *21*, 1448−1456.

(40) Heinen, M.; Chen, Y. X.; Jusys, Z.; Behm, R. J. In Situ ATR-FTIRS Coupled with On-Line DEMS under Controlled Mass Transport Conditions—A Novel Tool for Electrocatalytic Reaction Studies. *Electrochim. Acta* **2007**, *52*, 5634−5643.

(41) Wang, H.; Abruña, H. D. New Insights into Methanol and Formic Acid Electro-oxidation on Pt: Simultaneous DEMS and ATR-SEIRAS Study under Well-Defined Flow Conditions and Simulations of CO Spectra. *J. Chem. Phys.* **2022**, *156*, No. 034703.

(42) Wang, H.; Abruña, H. D. Identifying Adsorbed OH Species on Pt and Ru Electrodes with Surface-Enhanced Infrared Absorption Spectroscopy through CO Displacement. *J. Am. Chem. Soc.* **2023**, *145*, 18439−18446.

(43) Ramis, G.; Larrubia, M. A.; Busca, G. On the Chemistry of Ammonia over Oxide Catalysts: Fourier Transform Infrared Study of Ammonia, Hydrazine and Hydroxylamine Adsorption over Iron-Titania Catalyst. *Top. Catal.* **2000**, *11/12*, 161−166, DOI: 10.1023/A:1027246419307.

(44) Hall, J. R.; Hirons, D. A. Infrared and Raman Spectra of Magnus' Green Salt $[Pt(NH_3)_4][PtCl_4]$, and Its Deuterate. *Inorg. Chim. Acta* **1979**, *34*, L277−L279.

(45) Faggiani, R.; Howard-Lock, H. E.; Lock, C. J. L.; et al. Crystalline Structure and Vibrational Spectra of *cis*-Dichlorodiammine-*trans*-Dihydroxo-Platinum(IV), $PtCl_2(NH_3)_2(OH)_2$. *Can. J. Chem.* **1982**, *60*, 529−534.

(46) Nakamoto, K. *Infrared and Raman Spectra of Inorganic and Coordination Compounds, Part B: Applications in Coordination, Organometallic, and Bioinorganic Chemistry*, 6th ed.; John Wiley & Sons: Hoboken, NJ, 2009.

(47) Contour, J. P.; Pannetier, G. Hydrazine Decomposition over a Supported Iridium Catalyst. *J. Catal.* **1972**, *24*, 434−445.

(48) Suganuma, S.; Murakami, Y.; Ohyama, J.; Torikai, T.; Okumura, K.; Katada, N. Assignments of Bending Vibrations of Ammonia Adsorbed on Surfaces of Metal Oxides. *Catal. Lett.* **2015**, *145*, 1904−1912.

(49) Chen, X.; Zhang, T.; Zheng, M.; Wu, Z.; Wu, W.; Li, C. The Reaction Route and Active Site of Catalytic Decomposition of Hydrazine over Molybdenum Nitride Catalyst. *J. Catal.* **2004**, *224*, 473−478.

(50) Ramis, G.; Yi, L.; Busca, G. Ammonia Activation over Catalysts for the Selective Catalytic Reduction of NO_x and the Selective Catalytic Oxidation of NH_3. An FT-IR Study. *Catal. Today* **1996**, *28*, 373−380.

(51) Smimov, M. Y.; Gorodetskii, V. V.; Cholach, A. R. HREELS and TDS Studies of $NO+H_2$ and NH_3+O_2 Reactions on Pt(111). In *Fundamental Aspects of Heterogeneous Catalysis Studied by Particle Beams*; Brongersma, H. H.; van Santen, R. A., Eds.; Plenum Press: New York, 1991; pp 249−253.

(52) Kim, M.; Pratt, S. J.; King, D. A. In Situ Characterization of the Surface Reaction between Chemisorbed Ammonia and Oxygen on Pt{100}. *J. Am. Chem. Soc.* **2000**, *122*, 2409−2410.

(53) Brown, W. A.; King, D. A. NO Chemisorption and Reactions on Metal Surfaces: A New Perspective. *J. Phys. Chem. B* **2000**, *104*, 2578−2595.

(54) Morrow, B. A.; Cody, I. A. An Infrared Study of the Adsorption and Oxidation of Ammonia on Platinum. *J. Catal.* **1976**, *45*, 151−162.

(55) Ebbesen, S. D.; Mojet, B. L.; Lefferts, L. In Situ Attenuated Total Reflection Infrared (ATR-IR) Study of the Adsorption of NO_2^-, NH_2OH and NH_4^+ on Pd/Al_2O_3 and Pt/Al_2O_3. *Langmuir* **2008**, *24*, 869−879.

(56) Ling, Y.; Mills, C.; Weber, R.; Yang, L.; Zhang, Y. NMR, IR/Raman, and Structural Properties in HNO and RNO (R = Alkyl and Aryl) Metalloporphyrins with Implication for the HNO-Myoglobin Complex. *J. Am. Chem. Soc.* **2010**, *132*, 1583−1591.

(57) Koper, M. T. M.; van Santen, R. A.; Wasileski, S. A.; Weaver, M. J. Field-Dependent Chemisorption of Carbon Monoxide and Nitric Oxide on Platinum-Group (111) Surfaces: Quantum Chemical

Calculations Compared with Infrared Spectroscopy at Electrochemical and Vacuum-Based Interfaces. *J. Chem. Phys.* **2000**, *113*, 4392−4407.

(58) Weaver, M. J.; Zou, S.; Tang, C. A Concerted Assessment of Potential-Dependent Vibrational Frequencies for Nitric Oxide and Carbon Monoxide Adlayers on Low-Index Platinum-Group Surfaces in Electrochemical Compared with Ultrahigh Vacuum Environments: Structural and Electrostatic Implications. *J. Chem. Phys.* **1999**, *111*, 368−381.

(59) Hitchman, M. A.; Rowbottom, G. L. Transition Metal Nitrite Complexes. *Coord. Chem. Rev.* **1982**, *42*, 55−132.

(60) Bartram, M. E.; Windham, R. G.; Koel, B. E. Coadsorption of Nitrogen Dioxide and Oxygen on Pt(111). *Langmuir* **1988**, *4*, 240−246.

(61) Ueno, T.; Tanaka, H.; Sugawara, S.; Shinohara, K.; Ohma, A.; Hoshi, N.; Nakamura, M. Infrared Spectroscopy of Adsorbed OH on n(111)-(100) and n(111)-(111) Series of Pt Electrode. *J. Electroanal. Chem.* **2017**, *800*, 162−166.

(62) Durig, J. R.; Bush, S. F.; Nercer, E. E. Vibrational Spectrum of Hydrazine-d_4 and a Raman Study of Hydrogen Bonding in Hydrazine. *J. Chem. Phys.* **1966**, *44*, 4238−4247.

(63) Sacconi, L.; Sabatini, A. The Infra-Red Spectra of Metal(II)-Hydrazine Complexes. *J. Inorg. Nucl. Chem.* **1963**, *25*, 1389−1393.

(64) Alberas, D. J.; Kiss, J.; Liu, Z.-M.; White, J. M. Surface Chemistry of Hydrazine on Pt(111). *Surf. Sci.* **1992**, *278*, 51−61.

(65) Alluisetti, G. E.; Almaraz, A. E.; Amorebieta, V. T.; Doctorovich, F.; Olabe, J. A. Metal-Catalyzed Anaerobic Disproportionation of Hydroxylamine. Role of Diazene and Nitroxyl Intermediates in the Formation of N_2, N_2O, NO^+, and NH_3. *J. Am. Chem. Soc.* **2004**, *126*, 13432−13442.

(66) Bari, S. E.; Amorebieta, V. T.; Gutiérrez, M. M.; Olabe, J. A.; Doctorovich, F. Disproportionation of Hydroxylamine by Water-Soluble Iron(III) Porphyrinate Compounds. *J. Inorg. Biochem.* **2010**, *104*, 30−36.

(67) Nast, R.; Föppl, I. Über die Bildung von Hyponitrit durch Disproportionierung des Hydroxylamines. *Z. Anorg. Allg. Chem.* **1950**, *263*, 310−315.

(68) Hughes, M. N.; Shrimanker, K. Metal Complexes of Hydroxylamine. *Inorg. Chim. Acta* **1976**, *18*, 69−76.

(69) Hibbitts, D. D.; Jimenez, R.; Yoshimura, M.; Weiss, B.; Iglesia, E. Catalytic NO Activation and NO-H_2 Reaction Pathways. *J. Catal.* **2014**, *319*, 95−109.

(70) Figueiredo, M. C.; Hiltrop, D.; Sundararaman, R.; Schwarz, K. A.; Koper, M. T. M. Absence of Diffuse Double Layer Effect on the Vibrational Properties and Oxidation of Chemisorbed Carbon Monoxide on a Pt(111) Electrode. *Electrochim. Acta* **2018**, *281*, 127−132.

(71) Rodríguez, P.; Carcia, G.; Herrero, E.; Feliu, J. M.; Koper, M. T. M. Effect of the Surface Structure of Pt(100) and Pt(110) on the Oxidation of Carbon Monoxide in Alkaline Solution: an FTIR and Electrochemical Study. *Electrocatal* **2011**, *2*, 242−253.

(72) Garcia, G.; Rodriguez, P.; Rosca, V.; Koper, M. T. M. Fourier Tranform Infrared Spectroscopy Study of CO Electro-oxidation on Pt(111) in Alkaline Media. *Langmuir* **2009**, *25*, 13661−13666.

(73) Rodes, A.; Climent, V.; Orts, J.; Perez, J. M.; Pérez, J.; Aldaz, A. Nitric Oxide Adsorption at Pt(100) Electrode Surfaces. *Electrochim. Acta* **1998**, *44*, 1077−1090.

(74) Nakata, K.; Okubo, A.; Shimazu, K.; Yamakata, A.; Ye, S.; Osawa, M. Surface-Enhanced Infrared Absorption Spectroscopic Studies of Adsorbed Nitrate, Nitric Oxide and Related Compounds 1: Reduction of Adsorbed NO on a Platinum Electrode. *Langmuir* **2008**, *24*, 4352−4357.

(75) da Cunha, M. C. P. M.; Weber, M.; Nart, F. C. On the Adsorption and Reduction of NO_3^- Ions at Au and Pt Electrodes Studied by In Situ FTIR Spectroscopy. *J. Electroanal. Chem.* **1996**, *414*, 163−170, DOI: 10.1016/0022-0728(96)04697-9.

(76) Ishihara, T.; Eguchi, K.; Arai, H. An Infrared Study of NO Adsorbed on SiO_2-Supported Fe, Co, and Ni Bimetallic Alloy Catalysts for CO Hydrogenation. *Chem. Lett.* **1986**, *15*, 1695−1698.

(77) Nakamoto, K.; Fujita, J.; Murata, H. Infrared Spectra of Metallic Complexes. V. The Infrared Spectra of Nitro and Nitrito Complexes. *J. Am. Chem. Soc.* **1958**, *80*, 4817−4823.

(78) Hadjiivanov, K.; Bushev, V.; Kantcheva, M.; Klissurski, D. Infrared Spectroscopy Study of the Species Arising during NO_2 Adsorption on TiO_2 (Anatase). *Langmuir* **1994**, *10*, 464−471.

(79) Gatehouse, B. M. A Survey of the Infrared Spectra of NO_2 in Metal Complexes. *J. Inorg. Nucl. Chem.* **1958**, *8*, 79−86.

(80) Goebbert, D. J.; Garand, E.; Wende, T.; Bergmann, R.; Meijer, G.; Asmis, K. R.; Neumark, D. M. Infrared Spectroscopy of the Microhydrated Nitrate Ions $NO_3^-(H_2O)_{1-6}$. *J. Phys. Chem. A* **2009**, *113*, 7584−7592.

(81) Mihaylov, M. Y.; Zdravkova, V. R.; Ivanova, E. Z.; Aleksandrov, H. A.; Petkov, P. S.; Vayssilov, G. N.; Hadjiivanov, K. I. Infrared Spectra of Surface Nitrates: Revision of the Current Opinions Based on the Case Study of Ceria. *J. Catal.* **2021**, *394*, 245−258.

(82) Shih, M.-C.; Hsu, Y.-J.; Chu, L.-K. Infrared Spectroscopic and Kinetic Characterization on the Photolysis of Nitrite in Alcohol-Containing Aqueous Solutions. *J. Phys. Chem. A* **2020**, *124*, 3904−3914.

(83) Casero, E.; Alonso, C.; Martín-Gago, J. A.; Borgatti, F.; Felici, R.; Renner, F.; Lee, T.-L.; Zegenhagen, J. Nitric-Oxide Adsorption and Oxidation on Pt(111) in Electrolyte Solution under Potential Control. *Surf. Sci.* **2002**, *507−510*, 688−694.

(84) Lubezky, A.; Folman, M. Infrared Spectra of NO, N_2O, NO_2 and O_2 Adsorbed on SiO Films. *J. Chem. Soc., Faraday Trans. 1* **1978**, *74*, 2935−2941.

(85) Wang, H.; Löffler, T.; Baltruschat, H. Formation of Intermediates during Methanol Oxidation: A Quantitative DEMS Study. *J. Appl. Electrochem.* **2001**, *31*, 759−765.

(86) Zemlyanov, D. Y.; Smirnov, M. Y.; Gorodetskii, V. V.; Block, J. H. HREELS and TDS Studies of NO Adsorption and NO + H_2 Reaction on Pt(100) Surfaces. *Surf. Sci.* **1995**, *329*, 61−70.

(87) Cooper, J. N.; Chilton, J. E., Jr.; Powell, R. E. Reaction of Nitric Oxide with Alkaline Hydroxylamine. *Inorg. Chem.* **1970**, *9*, 2303−2304.

(88) Bonner, F. T.; Dzelzkalns, L. S.; Bonucci, J. A. Properties of Nitroxyl as Intermediate in the Nitric Oxide-Hydroxylamine Reaction and in Tri-oxodinitrate Decomposition. *Inorg. Chem.* **1978**, *17*, 2487−2494.

(89) Fehling, C.; Friedrichs, G. Dimerization of HNO in Aqueous Solution: An Interplay of Solvation Effects, Fast Acid-Base Equilibria, and Intramolecular Hydrogen Bonding? *J. Am. Chem. Soc.* **2011**, *133*, 17912−17922.

(90) Bhattacharyya, D.; Videla, P. E.; Cattaneo, M.; Batista, V. S.; Lian, T.; Kubiak, C. P. Vibrational Stark Shift Spectroscopy of Catalysts under the Influence of Electric Fields at Electrode-Solution Interfaces. *Chem. Sci.* **2021**, *12*, 10131−10149.

(91) Zou, S.; Weaver, M. J. Potential-Dependent Metal-Adsorbate Stretching Frequencies for Carbon Monoxide on Transition-Metal Electrodes: Chemical Bonding versus Electrostatic Field Effects. *J. Phys. Chem.* **1996**, *100*, 4237−4242.

(92) Farmer, P. J.; Sulc, F. Coordination Chemistry of the HNO Ligand with Hemes and Synthetic Coordination Complexes. *J. Inorg. Biochem.* **2005**, *99*, 166−184.

(93) Gland, J. L.; Korchak, V. N. Ammonia Oxidation on a Stepped Platinum Single-Crystal Surface. *J. Catal.* **1978**, *53*, 9−23.

(94) Mieher, W. D.; Ho, W. Thermally Activated Oxidation of NH_3 on Pt(111): Intermediate Species and Reaction Mechanisms. *Surf. Sci.* **1995**, *322*, 151−167.

(95) Il'chenko, N. I. Catalytic Oxidation of Ammonia. *Russ. Chem. Rev.* **1976**, *45*, 1119−1134.

(96) Katsounaros, I.; Figueiredo, M. C.; Chen, X.; Calle-Vallejo, F.; Koper, M. T. M. Structure- and Coverage-Sensitive Mechanism of NO Reduction on Platinum Electrodes. *ACS Catal.* **2017**, *7*, 4660−4667.

(97) Li, Z.-F.; Wang, Y.; Botte, G. G. Revisiting the Electrochemical Oxidation of Ammonia on Carbon-Supported Metal Nanoparticle Catalysts. *Electrochim. Acta* **2017**, *228*, 351−360.

(98) Wang, H.; Baltruschat, H. DEMS Study on Methanol Oxidation at Poly- and Single Crystalline Platinum Electrodes: the Effect of Anion, Temperature, Surface Structure, Ru Adatom and Potential. *J. Phys. Chem. C* **2007**, *111*, 7038−7048.

https://doi.org/10.1021/jacs.4c02621
J. Am. Chem. Soc. 2024, 146, 15926−15940